

1  
2  
3  
4 **Word count: 5891**  
5  
6

7 **Investigation of the properties of MgO recovered from reject brine obtained from**  
8 **desalination plants**  
9

10  
11 Haoliang Dong<sup>a</sup>, En-Hua Yang<sup>a</sup>, Cise Unluer<sup>a,\*</sup>, Fei Jin<sup>b</sup>, Abir Al-Tabbaa<sup>c</sup>  
12  
13

14 <sup>a</sup> School of Civil and Environmental Engineering, Nanyang Technological University, 50  
15 Nanyang Avenue, Singapore 639798, Singapore  
16

17 <sup>b</sup> School of Engineering, University of Glasgow, Glasgow G12 8QQ, United Kingdom

18 <sup>c</sup> Department of Engineering, University of Cambridge, Trumpington Street, Cambridge  
19 CB2 1PZ, United Kingdom  
20  
21  
22  
23

24 **Abstract**  
25  
26

27 In addition to its use in various applications such as those in the agriculture,  
28 pharmaceutical and refractory industries, MgO is being investigated as a cement binder  
29 due to the low calcination temperatures used during its production and its ability to gain  
30 strength by absorbing CO<sub>2</sub> in construction products. Similar to the dry-route, the  
31 reactivity of MgO synthesised from waste water or reject brine via the calcination of the  
32 precipitated Mg(OH)<sub>2</sub> depends on the calcination conditions. This study investigated the  
33 influence of two bases, namely ammonia solution (NH<sub>4</sub>OH) and sodium hydroxide  
34 (NaOH), on the properties of Mg(OH)<sub>2</sub> precipitated and consequently the characteristics  
35 of MgO produced under different calcination conditions. The energy consumption of the  
36 production of reactive MgO from reject brine via the addition of NH<sub>4</sub>OH and NaOH was  
37 also reported and compared with the industrial production routes to assess the  
38 sustainability of the production procedure. The final products were characterised in terms  
39 of their specific surface area (SSA) and microstructure. Results indicated that Mg(OH)<sub>2</sub>  
40 synthesised via the addition of NH<sub>4</sub>OH into reject brine generated a more porous, flake-  
41 like morphology than those obtained via the use of NaOH. The SSA and reactivity of  
42 NH<sub>4</sub>OH-based MgO demonstrated a sharper decrease with increasing temperature and  
43 duration compared to NaOH-based MgO. Out of all samples, NH<sub>4</sub>OH-based MgO  
44 calcined at 500 °C for 2 hours revealed the highest reactivity (SSA of 78.8 m<sup>2</sup>/g), which  
45 was higher than NaOH-based MgO (SSA of 51.4 m<sup>2</sup>/g).  
46  
47  
48  
49  
50  
51  
52  
53  
54  
55

56 **Keywords:** *Reject brine; MgO; cement; characterisation; reactivity*  
57  
58

---

59 \* Corresponding author. Address: N1-01c-74, 50 Nanyang Avenue, Singapore 639798. E-mail address:  
60 ucise@ntu.edu.sg (C. Unluer)  
61  
62  
63  
64  
65

1  
2  
3  
4 **1. Introduction**  
5  
6  
7

8 Magnesia (MgO) is an important material, which finds various uses in different  
9 applications within the refractory, agricultural, pharmaceutical, chemical and  
10 construction industries (Caraballo et al., 2009; Lee et al., 2004; Moussavi and Mahmoudi,  
11 2009a; Pilarska et al., 2017; Shand, 2006; Wang et al., 2016). The main production route  
12 for MgO involves the calcination of magnesite (i.e. dry-route), as shown in Equation 1.  
13 The second method is based on its synthesis from magnesium-rich sources such as  
14 seawater or brine (i.e. wet-route), as shown in Equations 2-4.  
15  
16  
17  
18  
19  
20  
21



26 The calcination conditions used during the production of MgO play a critical role as they  
27 determine the properties of the final product. Reactive MgO, produced at 700-1000 °C,  
28 through the dry-route, and at lower temperatures of around 500-700 °C through the wet-  
29 route, has a high specific surface area (SSA) and maintains a high level of reactivity.  
30 Increasing the calcination temperature any further reduces the SSA and reactivity of MgO.  
31 Unlike reactive MgO, hard- and dead-burned MgO are produced at > 1000 °C through  
32 the dry-route, thereby possessing relatively low SSA and reactivities. Within the  
33 construction industry, these MgO types are typically used in applications that exploit  
34 their expansive nature (e.g. as expansive agents in mass construction) (Gao et al., 2008;  
35 Mo et al., 2014) since their hydration rate is lower than those of reactive MgO or Portland  
36 cement (PC). Alternatively, the use of reactive MgO in cement-based formulations does  
37 not create any potential late expansion problems due to its similar hydration rate to PC  
38 (Dung and Unluer, 2017a; Dung and Unluer, 2017b).  
39  
40  
41  
42  
43  
44  
45  
46  
47  
48  
49  
50

51 In addition to the lower calcination temperatures used during their production (i.e. 700-  
52 1000 °C vs. 1450 °C for PC), reactive MgO-based binders are known to gain strength via  
53 carbonation, thereby enabling the permanent sequestration of carbon dioxide (CO<sub>2</sub>)  
54 within a range of construction products (Al-Tabbaa, 2013; Harrison, 2008; Liska et al.,  
55 2012a; Liska et al., 2012b; Unluer and Al-Tabbaa, 2013; Unluer and Al-Tabbaa, 2014).  
56  
57  
58  
59  
60  
61  
62  
63  
64  
65

1  
2  
3  
4 The strength gain mechanism of reactive MgO within cement-based applications involves  
5 its hydration to form Mg(OH)<sub>2</sub>, which then carbonates into a range of strength providing  
6 carbonate phases. During this process, the rate and the degree of these reactions, and  
7 hence strength gain, are controlled by many factors. One of the key factors influencing  
8 the strength and microstructural development of reactive MgO-based formulations is the  
9 reactivity of MgO, which is determined via its production parameters (Ruan and Unluer,  
10 2016).  
11  
12  
13  
14  
15  
16  
17  
18

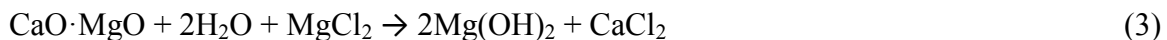
19 Other than magnesite and other Mg-bearing minerals which serve as a source for MgO  
20 through the dry-route, seawater contains an average Mg<sup>2+</sup> concentration of 1.29-1.35 g/L,  
21 thereby constituting a significant resource of magnesium (Boyd, 2015; Wright and  
22 Colling, 1995). Unlike the dry-route, the wet-route involves the precipitation of Mg(OH)<sub>2</sub>  
23 from the brine solution, which is then calcined to produced MgO. The characteristics of  
24 Mg(OH)<sub>2</sub>, such as its crystal size, shape and structure are strongly influenced by the type  
25 of solvent and base used during its production, and the pH and temperature of reaction, at  
26 the end of which Mg(OH)<sub>2</sub> with different morphologies (i.e. rod-, tube-, needle- and  
27 lamella-like etc.) can be obtained (Alvarado et al., 2000; Ding et al., 2001; Fan et al.,  
28 2004; Henrist et al., 2003; Wu et al., 2004; Yan et al., 2005).  
29  
30  
31  
32  
33  
34  
35  
36  
37  
38

39 Depending on the equilibrium constant values and dissociation degrees, a base, which  
40 releases OH<sup>-</sup> ions in an aqueous solution, can be categorized as a strong or weak base. An  
41 example to these base materials, sodium hydroxide (NaOH), introduced as an alkali  
42 source into MgCl<sub>2</sub> solutions, was found to produce Mg(OH)<sub>2</sub> with a globular,  
43 cauliflower-like morphology. Alternatively, the use of another base, ammonia (NH<sub>4</sub>OH),  
44 resulted in Mg(OH)<sub>2</sub> with a plate-like morphology, which was associated with the  
45 differences in the type of base and pH of the solution (Henrist et al., 2003). As the  
46 isoelectric point (IEP) of Mg(OH)<sub>2</sub> is situated at ~12, the higher pH induced by the  
47 addition of NaOH causes the surface to be negatively charged, where Na<sup>+</sup> derived from  
48 NaOH can easily be adsorbed without any selectivity. This mechanism hinders the  
49 attachment of Mg<sup>2+</sup> to the surface, resulting in its isotropic growth and aggregation that  
50 leads to the formation of a globular cauliflower-like morphology. By contrast, the  
51  
52  
53  
54  
55  
56  
57  
58  
59  
60  
61  
62  
63  
64  
65

1  
2  
3  
4 positively charged surface of particles due to the lower pH and IEP induced by NH<sub>4</sub>OH  
5 favours the adsorption of Mg<sup>2+</sup>. Furthermore, the larger size of NH<sub>4</sub><sup>+</sup> than Na<sup>+</sup>, which is  
6 not easily adsorbed on the crystal facets, results in the anisotropic growth of particles and  
7 thus the formation of a plate-like morphology.  
8  
9

10  
11  
12  
13 Reject brine, a concentrated by-product obtained from treating brackish water or seawater  
14 in desalination plants, has a great potential to be used as an MgO source due to its high  
15 Mg<sup>2+</sup> content (i.e. 30% more than seawater) and abundance on both local and global  
16 levels. It is estimated that the world production of desalination water exceeds 30 million  
17 m<sup>3</sup>/day, which generates an equivalent amount of reject brine (El-Naas, 2011). The  
18 highly saline effluent brine from the desalination process not only has no economic value,  
19 but also has adverse effects on the marine ecosystem as it is currently discharged back  
20 into the sea. This process disturbs the local water and sediment by introducing a multi-  
21 component waste and increasing the temperature, also endangering the marine organisms  
22 due to the residual chemicals mixed into the brine from the pre-treatment process.  
23 Production of MgO from reject brine provides a new purpose for this otherwise harmful  
24 waste material and proposes a potentially sustainable alternative for the current  
25 production of MgO.  
26  
27  
28  
29  
30  
31  
32  
33  
34  
35  
36  
37  
38

39 The extraction of MgO from reject brine involves the use of a base, such as slaked lime  
40 (Ca(OH)<sub>2</sub>), dolime (CaO·MgO), NaOH or NH<sub>4</sub>OH to enable the precipitation of  
41 Mg(OH)<sub>2</sub> in the first stage (Dave and Ghosh, 2005; Khuyen Thi et al., 2016; Tran et al.,  
42 2013; Turek and Gnot, 1995). The obtained Mg(OH)<sub>2</sub> is then heated to around 400-  
43 500 °C, leading to the production of MgO, as illustrated in Equations 2-4.  
44  
45  
46  
47  
48  
49



53  
54  
55  
56  
57 The parameters that influence the properties of MgO obtained via the calcination of  
58 MgCO<sub>3</sub> or Mg(OH)<sub>2</sub> have been reported by several studies (Alvarado et al., 2000; Bartley  
59  
60  
61

1  
2  
3  
4 et al., 2012; Choudhary et al., 1994; Eubank, 1951; Itatani et al., 1988; Mo et al., 2010).  
5  
6 The main parameters that control the properties of the final product have been identified  
7  
8 as calcination conditions (i.e. temperature and duration), as well as the characteristics of  
9  
10 the precursor (i.e. physical properties and chemical composition). Accordingly, the  
11  
12 decomposition temperature of  $\text{MgCO}_3$  is between 400 and 750 °C, which depends on its  
13  
14 impurity level, crystallographic structure, microstructure and production conditions  
15  
16 (Boynton, 1980; Knibbs, 1924; Shand, 2006). Increasing the calcination temperature and  
17  
18 duration decreases the SSA and hence the reactivity of MgO (Mo et al., 2010), thereby  
19  
20 controlling its performance in various applications.  
21

22  
23 The feasibility of producing MgO with a high reactivity from reject brine via the addition  
24  
25 of  $\text{NH}_4\text{OH}$  and  $\text{NaOH}$  has been presented in previous studies (Dong et al., 2017; Dong et  
26  
27 al., 2018). One of the main factors determining the efficiency of the overall synthesis was  
28  
29 the type and amount of the base introduced into the reject brine. Accordingly, the  
30  
31 characteristics of  $\text{Mg}(\text{OH})_2$  and resulting MgO significantly varied under the use of  
32  
33 different bases, especially in terms of reactivity and microstructure. However, the  
34  
35 influence of base type, and reaction and calcination conditions on the textural properties  
36  
37 (i.e. SSA and pore size distribution) and reactivity of the MgO obtained from reject brine  
38  
39 has not been revealed yet.  
40

41  
42 For the accurate characterization of the final product, the relationship between these key  
43  
44 parameters (i.e. base type and reaction/calcination conditions) on the properties of MgO  
45  
46 must be thoroughly comprehended. Establishing clear links between the production  
47  
48 conditions and final properties of MgO will enable its effective use and the identification  
49  
50 of the right applications in line with its capabilities. With this goal in mind, this paper  
51  
52 presents a comprehensive characterization of MgO obtained via the calcination of  
53  
54  $\text{Mg}(\text{OH})_2$  precipitated using two different bases ( $\text{NH}_4\text{OH}$  and  $\text{NaOH}$ ) and compares the  
55  
56 properties of the final product produced under different calcination conditions. The  
57  
58 obtained results shed a light on the influence of different base environments and  
59  
60 calcination conditions on the properties of MgO and highlighted potential application  
61  
62 areas that can benefit from the end product. The energy consumption of the production of  
63  
64  
65

reactive MgO from reject brine via the addition of NaOH and NH<sub>4</sub>OH was also reported and compared with the industrial production of MgO from seawater/brine and the dry-route to evaluate the utilization of reject brine from a sustainability standpoint.

## 2. Materials and Methodology

### 2.1. Materials

Reject brine, whose cation composition obtained via inductively coupled plasma-optical emission spectroscopy (ICP-OES) is listed in Table 1, was provided by a local desalination plant in Singapore. Ammonium hydroxide solution (NH<sub>4</sub>OH with 25% NH<sub>3</sub> content) and sodium hydroxide (NaOH), used as the alkaline sources in the synthesis of Mg(OH)<sub>2</sub>, were supplied by Sigma-Aldrich and VWR Pte Ltd in Singapore, respectively.

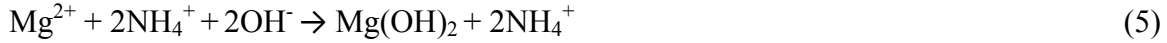
Table 1 Chemical composition of reject brine used in this study

Element/ Concentration	Cl	Na	SO <sub>4</sub>	Mg	K	Ca	Sr	B	Si	Li	P	Al
ppm	65593.	16124.	4322.	1679.	808.	563.	5.	4.	0.	0.	0.	0.
	1	3	6	0	5	6	3	5	5	4	2	1

### 2.2. Methodology

The first step involved the synthesis of Mg(OH)<sub>2</sub> from reject brine via the addition of the bases, in line with the procedure explained in detail in previous studies (Dong et al., 2017; Dong et al., 2018). NH<sub>4</sub>OH was included at a NH<sub>4</sub>OH/Mg<sup>2+</sup> molar ratio of 6, whereas NaOH was added at a NaOH/Mg<sup>2+</sup> molar ratio of 2 to achieve Mg(OH)<sub>2</sub> with the highest purity and yield, as optimized in the aforementioned previous studies. Mg(OH)<sub>2</sub> that precipitated at the end of the reactions shown in Equations 5 and 6 was calcined to

1  
2  
3  
4 produce MgO. The calcination process involved the heating of Mg(OH)<sub>2</sub> at a rate of  
5  
6 10 °C/min to reach three different calcination temperatures (500, 600 and 700 °C), which  
7  
8 were each maintained for three different residence times (2, 6 and 12 hours).  
9



14  
15  
16  
17 As a detailed analysis and characterization of Mg(OH)<sub>2</sub> obtained via the reaction of reject  
18  
19 brine with NH<sub>4</sub>OH and NaOH was presented earlier (Dong et al., 2017; Dong et al.,  
20  
21 2018), this study mainly focused on the characterization and comparison of the final  
22  
23 product, MgO, obtained via the use of two distinct bases under different calcination  
24  
25 conditions. A Bruker D8 Advance with a Cu K $\alpha$  source was used to perform X-ray  
26  
27 powder diffraction (XRD) under the operation conditions of 40 kV and 40 mA, emitting  
28  
29 radiation with a wavelength of 1.5405 Å, scan rate of 0.02 °/step, and a 2 $\theta$  range of 5 to  
30  
31 70°. The microstructures of the solids were analysed by imaging powder surface via a  
32  
33 JSM-7600F thermal field emission scanning electron microscopy (FESEM), operated  
34  
35 under a vacuum condition of 2.5×10<sup>-3</sup> Pa and 2 kV. The thermo-properties of the final  
36  
37 phases were characterized via thermogravimetric and differential thermal analysis  
38  
39 (TG/DTA) using a PyrisDiamond TGA 4000 operated at a heating rate of 10 °C/min  
40  
41 under air flow. The texture properties, namely SSA and pore volume, were determined  
42  
43 from nitrogen adsorption-desorption isotherms using a Quadrasorb Evo automated  
44  
45 surface area and pore size analyser. The SSA was calculated by Brunauer-Emmett-Teller  
46  
47 (BET) method, while the pore volume was determined by Barrett-Joyner-Halenda (BJH)  
48  
49 method. The reactivity of MgO was tested via the measurement of the time required to  
50  
51 neutralize an acid solution with a phenolphthalein pH indicator. This acid reactivity test  
52  
53 involved the use of 0.28 grams of synthesized MgO, which was added into 50 ml of 0.07  
54  
55 mol/L citric acid solution (Mo et al., 2010; Shand, 2006).  
56  
57  
58  
59  
60  
61  
62  
63  
64  
65

66  
67 The agglomeration ratio, defined as G<sub>BET</sub>/G<sub>XRD</sub>, involved the calculation of the primary  
68  
69 particle size (G<sub>BET</sub>), which was obtained from the SSA and crystallite size. G<sub>BET</sub> was  
70  
71 calculated according to the equation G<sub>BET</sub> = F/ρS, where F is the particle-shape factor (6),  
72  
73  
74  
75

1  
2  
3  
4 S is the SSA ( $\text{m}^2/\text{g}$ ) and  $\rho$  is the theoretical density of MgO ( $3.595 \text{ g/cm}^3$ ) (Itatani et al.,  
5 1986). The crystallite size ( $G_{\text{XRD}}$ ) was calculated according to  $G_{\text{XRD}} = K \cdot \lambda / (\beta \cdot \cos(\theta))$ ,  
6 where  $\lambda$  is the wavelength of Cu  $K\alpha$  ( $1.5405 \text{ \AA}$ ),  $\beta$  is the full width at half-maximum  
7 intensity (FWHM) of a Bragg reflection subtracting the instrumental broadening,  $\theta$  is the  
8 Bragg angle and K is the shape factor with a typical value as 0.9 (Patterson, 1939).  
9  
10  
11  
12  
13  
14  
15  
16

### 17 **3. Results and Discussions**

#### 18 19 20 **3.1. Characterization of Mg(OH)<sub>2</sub>**

##### 21 22 **3.1.1. Composition and textural properties**

23  
24  
25  
26  
27  
28 Figure 1 shows the XRD diffractograms of the synthesized Mg(OH)<sub>2</sub> obtained via the  
29 reaction between reject brine and two different base solutions involving the use of  
30 NH<sub>4</sub>OH and NaOH. The two diffraction patterns presented similar phases, which were  
31 mainly attributed to Mg(OH)<sub>2</sub>, along with minor amounts of CaCO<sub>3</sub> in the crystal form of  
32 aragonite. As discussed in previous studies (Dong et al., 2017; Dong et al., 2018), the  
33 elevated molar ratios of NH<sub>4</sub>OH/Mg<sup>2+</sup> and NaOH/Mg<sup>2+</sup> lead to a shift in the crystal  
34 structure of CaCO<sub>3</sub> from aragonite to calcite without changing the properties of Mg(OH)<sub>2</sub>.  
35 Regardless of the base material used, as the main goal was to determine the optimum  
36 ratios that led to the production of Mg(OH)<sub>2</sub> and subsequently MgO with the highest  
37 purity and yield via each reaction path, the molar ratios of NH<sub>4</sub>OH/Mg<sup>2+</sup> and NaOH/Mg<sup>2+</sup>  
38 were determined as 6 and 2, respectively. Although two different ratios were used for  
39 each base material, the composition of Mg(OH)<sub>2</sub> synthesized via the use of these different  
40 base solutions did not differ and resulted in a similarly high purity level of ~94% for both  
41 cases, as detailed in Table 2, along with other textural properties.  
42  
43  
44  
45  
46  
47  
48  
49  
50  
51  
52

53  
54  
55 In addition to the purity level, the crystallite size of both samples was calculated  
56 according to the Debye-Scherrer formula. The major characteristic peak of Mg(OH)<sub>2</sub> at  
57 38.1°  $2\theta$  was used in this calculation. NH<sub>4</sub>OH- and NaOH-based Mg(OH)<sub>2</sub> possessed a  
58  
59  
60  
61  
62  
63  
64  
65



crystallite size of 15.4 and 10.5 nm, respectively. The differences in the crystallite sizes of both samples could be associated with the different strengths of  $\text{NH}_4\text{OH}$  and  $\text{NaOH}$  as a base and the chemical nature of ions present in the solution.  $\text{NaOH}$ , which is a strong base, ionizes completely and produces a significant number of  $\text{OH}^-$  once dissolved in water. On the other hand,  $\text{NH}_4\text{OH}$  is a weaker base and electrolyte, which only ionizes to a limited extent in water, gradually releasing  $\text{OH}^-$  into the solution. The higher concentration of  $\text{OH}^-$  provided by  $\text{NaOH}$  could accelerate the reaction of  $\text{Mg}^{2+}$  with  $\text{OH}^-$ , thereby enhancing the formation of  $\text{Mg}(\text{OH})_2$  crystals and resulting in a shorter reaction time. The elevated pH value created a high supersaturation level, which formed a larger amount of particles and generated a faster nucleation process, and hence smaller crystals (Markov, 2016).

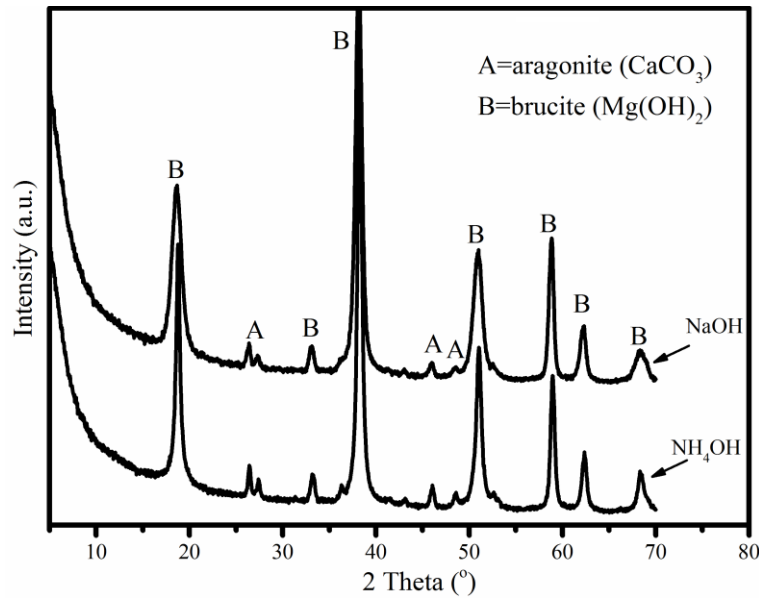


Figure 1 XRD diffractograms of  $\text{Mg}(\text{OH})_2$  obtained from the reaction of reject brine with  $\text{NH}_4\text{OH}$  and  $\text{NaOH}$  (Dong et al., 2017; Dong et al., 2018)

Table 2 Chemical composition, crystallite size, SSA and pore volume of  $\text{Mg}(\text{OH})_2$  obtained from the reaction of reject brine with  $\text{NH}_4\text{OH}$  and  $\text{NaOH}$

Base	Phase contents (%)		$G_{\text{XRD}}$ (nm)	SSA ( $\text{m}^2/\text{g}$ )	Pore volume ( $\text{cm}^3/\text{g}$ )
	$\text{Mg}(\text{OH})_2$	$\text{CaCO}_3$			
$\text{NH}_4\text{OH}$	93.5	6.5	15.4	10.6	0.055

NaOH	93.7	6.3	10.5	7.4	0.029
------	------	-----	------	-----	-------

---

### 3.1.2. Microstructure

The morphology of  $\text{Mg}(\text{OH})_2$  obtained via the addition of  $\text{NH}_4\text{OH}$  and  $\text{NaOH}$  to reject brine was further investigated through FESEM, as shown in Figure 2. The use of  $\text{NaOH}$  generated a densely packed granular morphology with relatively clear boundaries. Alternatively, those produced via the use of  $\text{NH}_4\text{OH}$  demonstrated a flake-like morphology with a more porous structure, which was in line with the findings of previous studies (Henrist et al., 2003).

These microstructural observations were confirmed by BET results that revealed the SSA of  $\text{Mg}(\text{OH})_2$  produced through these two distinct routes. As shown in Table 2,  $\text{NH}_4\text{OH}$ - and  $\text{NaOH}$ -based  $\text{Mg}(\text{OH})_2$  possessed a SSA of 10.6 and 7.4  $\text{m}^2/\text{g}$ , respectively. Furthermore, the pore volumes of both samples were recorded as 0.055 and 0.029  $\text{cm}^3/\text{g}$ , respectively. This morphological difference could be related to the pH and cations present in each solution (Hanlon et al., 2015; Henrist et al., 2003). The introduction of the strong base,  $\text{NaOH}$ , set the pH of solution beyond the IEP of  $\text{Mg}(\text{OH})_2$  (~12) (Hanlon et al., 2015). Furthermore, the high supersaturation generated by  $\text{NaOH}$  enhanced the nucleation of tiny crystals, which agglomerated together and generated a much denser structure with a lower porosity, therefore resulting in a lower SSA. On the other hand, the addition of the weaker base,  $\text{NH}_4\text{OH}$ , favoured the binding of  $\text{OH}^-$  to the basal plane, leading to anisotropic growth and hence the formation of a flake-like structure.

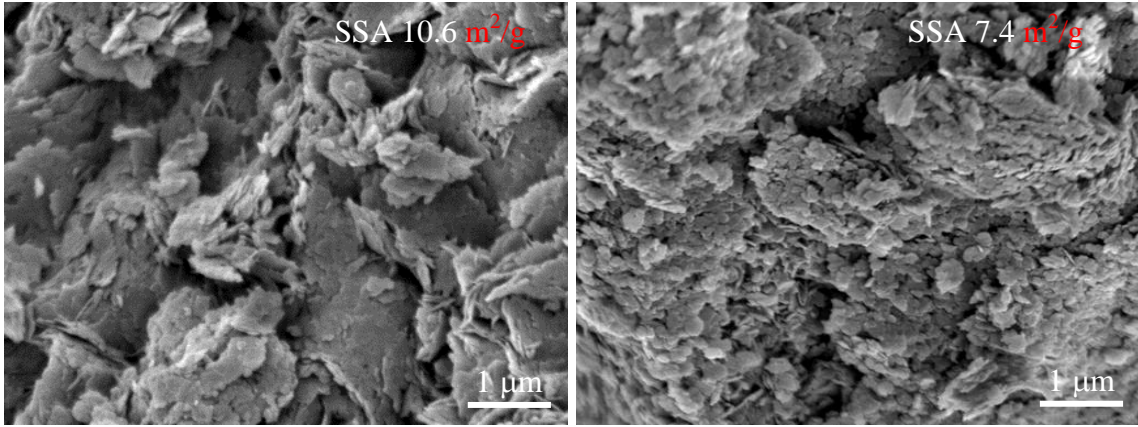


Figure 2 FESEM images of Mg(OH)<sub>2</sub> obtained from the reaction of reject brine with (a) NH<sub>4</sub>OH and (b) NaOH (Dong et al., 2017; Dong et al., 2018)

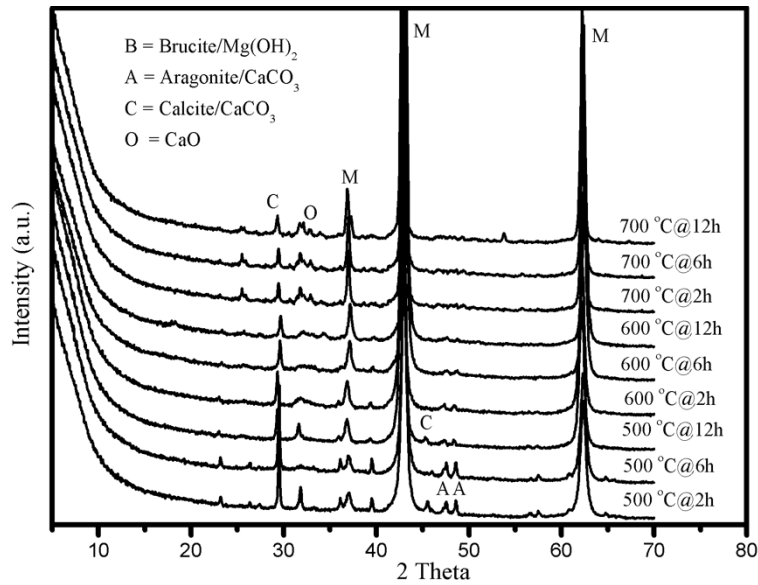
### 3.2. Characterization of MgO

#### 3.2.1. Composition

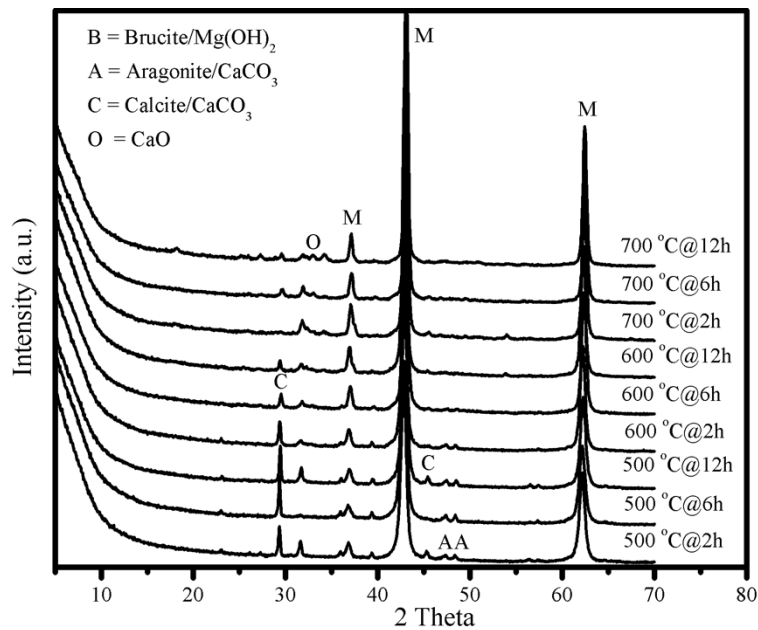
The XRD patterns of MgO, obtained from the calcination of Mg(OH)<sub>2</sub>, generated via the reaction of reject brine with NH<sub>4</sub>OH and NaOH, under different calcination conditions are shown in Figures 3(a) and 3(b), respectively. In both cases, Mg(OH)<sub>2</sub> was completely decomposed into MgO under the calcination conditions studied (i.e. 500-700 °C for 2-12 hours). The characteristic peaks of MgO, which were located at 37.0°, 43.1° and 62.3° 2θ, matched well with the reference peaks of MgO indicated in JCPDS card no. 89-7746. Along with MgO, a few minor peaks attributed to CaCO<sub>3</sub> and CaO were observed in the XRD patterns of all samples.

Aragonite (primary peaks at 47.5° and 48.6° 2θ), which was initially present within the sample composition, gradually transformed into calcite (primary peaks at 29.5° and 43.1° 2θ) at higher calcination temperatures (600 °C). This was because aragonite is known to convert to calcite, which possesses a higher entropy and is more stable, at temperatures above 400 °C (Kontoyannis and Vagenas, 2000). The clear reduction in the intensity of the calcite peak at 29.5° 2θ indicated the decomposition of CaCO<sub>3</sub> into CaO as the

1  
2  
3  
4 calcination temperature further increased to 700 °C. The overall results demonstrated the  
5  
6 similar phase transitions of NH<sub>4</sub>OH- and NaOH-based samples under increasing  
7  
8 calcination temperatures and durations, which were in line with the findings reported  
9  
10 earlier (Dong et al., 2017; Dong et al., 2018). These outcomes highlighted that, albeit  
11  
12 their similar compositions, the final products differed in terms of their physical properties  
13  
14 and morphology, which were determined by the production parameters.  
15  
16



(a)



(b)

1  
2  
3  
4 Figure 3 XRD diffractograms of reactive MgO obtained from the calcination of Mg(OH)<sub>2</sub>  
5 that was synthesized via the reaction of reject brine with (a) NH<sub>4</sub>OH and (b) NaOH,  
6  
7 under different calcination temperatures and durations  
8  
9

### 10 11 12 13 **3.2.2. Textural properties** 14

15  
16  
17 The SSA values of MgO, obtained from the calcination of Mg(OH)<sub>2</sub> generated via the  
18 reaction of reject brine with NH<sub>4</sub>OH and NaOH under different calcination conditions  
19 (i.e. temperature and duration), are displayed in Figure 4. The data on the production of  
20 MgO at 500 °C for 2 hours were taken from previous studies (Dong et al., 2017; Dong et  
21 al., 2018). The SSA values ranged between 5.5 and 78.8 m<sup>2</sup>/g, depending on the base  
22 used and the calcination conditions. An increase in the calcination temperature and  
23 duration led to a consistent reduction in SSA, indicating a decrease in the reactivity of  
24 both NH<sub>4</sub>OH- and NaOH-based MgO samples, whose details are listed in Table 3. The  
25 calcination of Mg(OH)<sub>2</sub> involved the release of H<sub>2</sub>O from Mg(OH)<sub>2</sub>, resulting in MgO  
26 with a porous structure. Increasing the calcination temperature beyond the decomposition  
27 point of Mg(OH)<sub>2</sub> led to the sintering of MgO, breaking down the pores in MgO and  
28 causing a reduction in its porosity, thereby increasing its crystallite size (Eubank, 1951).  
29 These findings were in line with those reported in previous studies (Alvarado et al., 2000;  
30 Eubank, 1951; Itatani et al., 1988; Jin and Al-Tabbaa, 2014; Mo et al., 2010), where the  
31 direct influence of calcination conditions on the properties of the final product was  
32 reported.  
33  
34  
35  
36  
37  
38  
39  
40  
41  
42  
43  
44  
45  
46  
47

48 Out of all conditions used in this study, the calcination of NH<sub>4</sub>OH-based Mg(OH)<sub>2</sub> under  
49 500 °C for 2 hours generated the highest SSA of 78.8 m<sup>2</sup>/g, while NaOH-based samples  
50 led to corresponding SSA values of 51.4 m<sup>2</sup>/g. Compared with NaOH-based MgO,  
51 NH<sub>4</sub>OH-based MgO achieved higher SSA values at lower calcination temperatures (500  
52 °C). This could be due to the difference in the textural properties of the precursor,  
53 Mg(OH)<sub>2</sub> (i.e. NH<sub>4</sub>OH-based Mg(OH)<sub>2</sub> possessed a higher SSA and porosity than NaOH-  
54 based Mg(OH)<sub>2</sub>). Accordingly, the calcination of NH<sub>4</sub>OH-based Mg(OH)<sub>2</sub> generated  
55  
56  
57  
58  
59  
60  
61  
62  
63  
64  
65

1  
2  
3  
4 MgO samples with a more porous structure and thereby higher SSA values that  
5 corresponding NaOH-based samples at lower calcination temperatures, as shown in  
6 Figure 4.  
7  
8  
9

10  
11 This trend reversed as the calcination temperature increased from 500 to 700 °C,  
12 indicating a sharp decline in the SSA and porosity of NH<sub>4</sub>OH-based MgO, whereas the  
13 SSA of NaOH-based MgO was not affected at the same rate. At the highest calcination  
14 temperature of 700 °C, NaOH-based samples revealed higher SSA and porosity values  
15 than NH<sub>4</sub>OH-based ones (SSA of 24.8 vs. 10.3 m<sup>2</sup>/g; porosity of 0.160 vs. 0.041 cm<sup>3</sup>/g),  
16 which was especially apparent at shorter residence times (2 and 6 hours). When  
17 compared to NaOH-based samples, the porous structures of NH<sub>4</sub>OH-based samples  
18 demonstrated a larger reduction in SSA associated with the rapid growth of MgO grains.  
19 These differences in SSA values could be attributed to the initially highly porous  
20 structure of NH<sub>4</sub>OH-based samples, which were more influenced under elevated  
21 calcination conditions. These results indicated that the critical temperature for the  
22 sintering of NH<sub>4</sub>OH-based Mg(OH)<sub>2</sub> was lower than that of NaOH-based Mg(OH)<sub>2</sub>,  
23 which caused the SSA trend to reverse at higher temperature ranges (Eubank, 1951).  
24  
25  
26  
27  
28  
29  
30  
31  
32  
33  
34  
35  
36

37 Similar to the calculation of the crystallite size of Mg(OH)<sub>2</sub> that was explained earlier, the  
38 major characteristic peak of MgO at 43.1° 2θ was used in the determination of its  
39 crystallite size ( $G_{XRD}$ ), which ranged between 10 and 25 nm for both NH<sub>4</sub>OH- and  
40 NaOH-based samples. The  $G_{BET}$  values for NH<sub>4</sub>OH- and NaOH-based MgO samples  
41 were in the range of 20-350 nm, while the agglomeration ratio ( $G_{BET}/G_{XRD}$ ) ranged  
42 between 1.7 and 16.3. The lowest agglomeration ratio of 1.7 was revealed by the  
43 NH<sub>4</sub>OH-based sample that was obtained under the calcination conditions of 500 °C for 2  
44 hours. In line with their effect on the SSA of MgO, calcination temperature and duration  
45 also had a significant influence on the crystallite size and primary size of MgO, which  
46 increased with increasing temperature and duration, regardless of the base utilized. This  
47 could be due to the spontaneous coagulation of primary particles under high temperatures  
48 and durations (Itatani et al., 1993). Compared with NH<sub>4</sub>OH-based samples, NaOH-based  
49  
50  
51  
52  
53  
54  
55  
56  
57  
58  
59  
60  
61  
62  
63  
64  
65

MgO samples generally achieved higher agglomeration ratios, which could explain the differences in their SSA values, as illustrated in Figure 4.

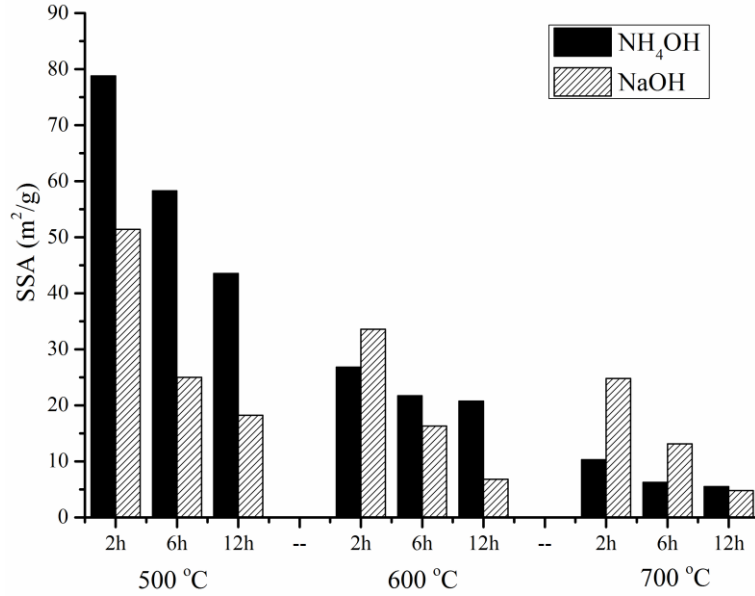


Figure 4 SSA of MgO produced under different calcination temperatures and durations

Table 3 Crystallite size, primary size and pore volume of MgO produced under different calcination temperatures and durations

Base	500 °C			600 °C			700 °C			
	2 h	6 h	12 h	2 h	6 h	12 h	2 h	6 h	12 h	
NH <sub>4</sub> OH	$G_{XRD}$ (nm)	12.6	13.4	14.8	15.5	16.1	17.9	19.5	24.7	24.9
	$G_{BET}$ (nm)	21.2	28.6	38.3	62.3	76.9	80.4	162.0	267.0	303.5
	$G_{BET}/G_{XRD}$	1.7	2.1	2.6	4.0	4.8	4.5	8.3	10.8	12.2
	Pore volume (cm <sup>3</sup> /g)	0.445	0.371	0.240	0.157	0.117	0.109	0.041	0.029	0.016
NaOH	$G_{XRD}$ (nm)	11.4	12.7	13.6	15.0	16.7	18.1	18.9	19.4	21.4
	$G_{BET}$ (nm)	32.5	66.8	91.7	49.7	102.4	245.4	67.3	127.4	347.7
	$G_{BET}/G_{XRD}$	2.8	5.3	6.8	3.3	6.1	13.6	3.6	6.6	16.3
	Pore volume (cm <sup>3</sup> /g)	0.317	0.16	0.083	0.166	0.058	0.024	0.160	0.056	0.017

1  
2  
3  
4  
5  
6  
7  
8  
9  
10  
11  
12  
13  
14  
15  
16  
17  
18  
19  
20  
21  
22  
23  
24  
25  
26  
27  
28  
29  
30  
31  
32  
33  
34  
35  
36  
37  
38  
39  
40  
41  
42  
43  
44  
45  
46  
47  
48  
49  
50  
51  
52  
53  
54  
55  
56  
57  
58  
59  
60  
61  
62  
63  
64  
65

---

volume  
(cm<sup>3</sup>/g)

---

### 3.2.3. Reactivity

Figure 5 shows the acid reactivity of MgO, obtained from the calcination of Mg(OH)<sub>2</sub>, generated via the reaction of reject brine with NH<sub>4</sub>OH and NaOH, under different calcination conditions (Dong et al., 2018). An increase in the neutralization time with an increase in the temperature and duration was observed in all cases, which was an indication of the reduction in reactivity. These findings highlighting the decline in the reaction rate of MgO under elevated calcination conditions were in line with those reported in earlier studies (Jin and Al-Tabbaa, 2014; Mo et al., 2010).

Amongst the two different bases used, NH<sub>4</sub>OH-based MgO samples revealed shorter neutralization times in comparison to NaOH-based ones produced under lower calcination temperatures (500 °C). An increase in the calcination temperature from 500 to 700 °C caused a notable increase in the neutralization times of NH<sub>4</sub>OH-based samples, during which those of NaOH-based samples demonstrated a gradual increase. These trends were in line with the SSA measurements reported earlier in Figure 4, where it was shown that the initially high SSA of NH<sub>4</sub>OH-based samples demonstrated a sharp decrease with increasing calcination temperatures.

The influence of calcination conditions and base type on the properties of MgO was also revealed via a comparison of the SSA and neutralization time (i.e. acid reactivity) of all the samples, as shown in Figure 6 (Dong et al., 2018). The inverse correlation between SSA and neutralization time could be clearly observed in all MgO samples, regardless of the utilized base type. Accordingly, higher SSA values corresponded to shorter neutralization times, which was an indication of the higher reactivity of MgO. Alternatively, lower SSA led to longer neutralization times associated with the lower reactivity and slower reaction of MgO. Although the acid reactivity test could not fully



distinguish amongst MgO samples with high SSA values ( $> 40 \text{ m}^2/\text{g}$ ) as the neutralization time demonstrated by these samples were relatively short, the obtained results clearly indicated the relationship between the two parameters, highlighting the importance of production conditions on the properties of the final product.

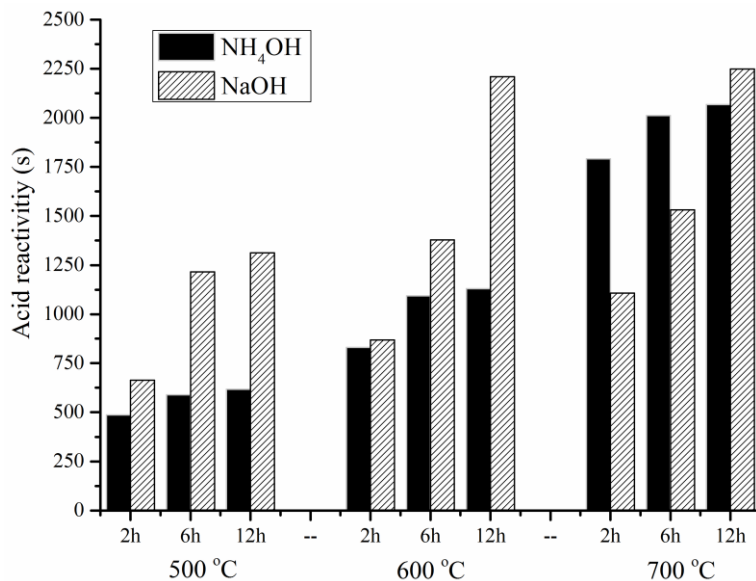


Figure 5 Effect of calcination temperature and duration on the neutralization time of reactive MgO

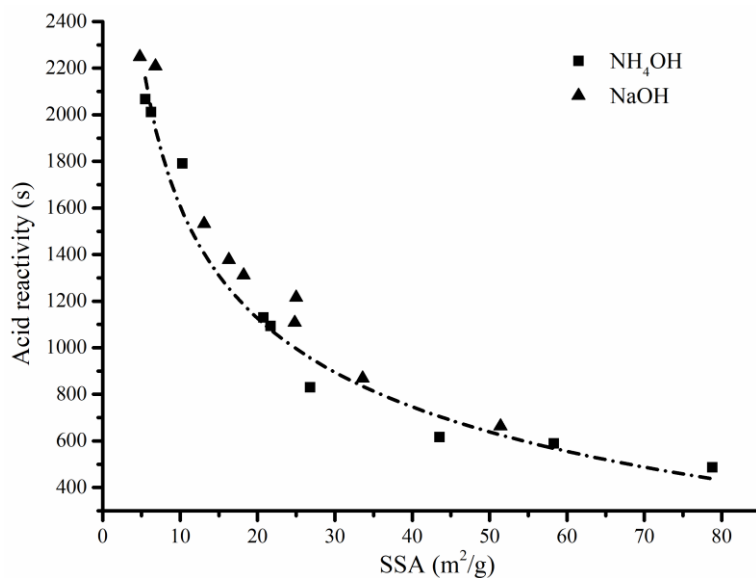


Figure 6 Relationship between the neutralization time (reactivity) and SSA of MgO

#### 3.2.4. Microstructure

A further investigation on the influence of the calcination conditions (i.e. temperature and duration) and base type (i.e.  $\text{NH}_4\text{OH}$  and  $\text{NaOH}$ ) on the morphology of the final product ( $\text{MgO}$ ) was revealed through FESEM, as shown in Figures 7 and 8. A single particle of  $\text{MgO}$  consisted of layered grains, which were inherited from the parent material,  $\text{Mg}(\text{OH})_2$ . Increasing the calcination temperature from 500 to 700 °C had a profound effect on the size of the  $\text{MgO}$  grains, resulting in a significant growth in crystallite size, which was accompanied with a reduction in porosity, as seen in Figures 7(a)-(c). The effect of the calcination duration on the morphology of  $\text{MgO}$  was revealed in Figures 7(c)-(e), for which the calcination duration increased from 2 to 12 hours. Production of  $\text{MgO}$  under longer calcination durations led to a noticeable growth in the size of grains. These changes in the morphology of  $\text{MgO}$  grains could clearly explain the reduction of its SSA and the corresponding increase in neutralization time (i.e. decrease of reactivity) under elevated calcination temperatures and durations.

A comparison of Figures 7(a) and 8(a) revealed the porous structure of  $\text{NH}_4\text{OH}$ -based  $\text{MgO}$  in comparison to  $\text{NaOH}$ -based samples, which were both produced under 500 °C for 2 hours. Increasing the calcination temperature and duration to 700 °C for 12 hours led to an increase in the size of  $\text{NH}_4\text{OH}$ -based  $\text{MgO}$  grains, whose growth was much more noticeable than those observed in  $\text{NaOH}$ -based samples ( $G_{\text{XRD}}$  of 24.9 vs. 21.4 nm, listed in Table 3), as demonstrated in Figures 7(e) and 8(b). The increase in the dimensions of the  $\text{MgO}$  grains under high calcination temperatures and durations was attributed to the loss of water during the decomposition of  $\text{Mg}(\text{OH})_2$ , which facilitated the formation of a porous structure. This initial porosity was gradually reduced as the  $\text{MgO}$  grains grew further due to continuous sintering, which was in line with the measurements revealed earlier in Table 3 and findings reported by earlier studies (Mo et al., 2010).

1  
2  
3  
4  
5  
6  
7  
8  
9  
10  
11  
12  
13  
14  
15  
16  
17  
18  
19  
20  
21  
22  
23  
24  
25  
26  
27  
28  
29  
30  
31  
32  
33  
34  
35  
36  
37  
38  
39  
40  
41  
42  
43  
44  
45  
46  
47  
48  
49  
50  
51  
52  
53  
54  
55  
56  
57  
58  
59  
60  
61  
62  
63  
64  
65

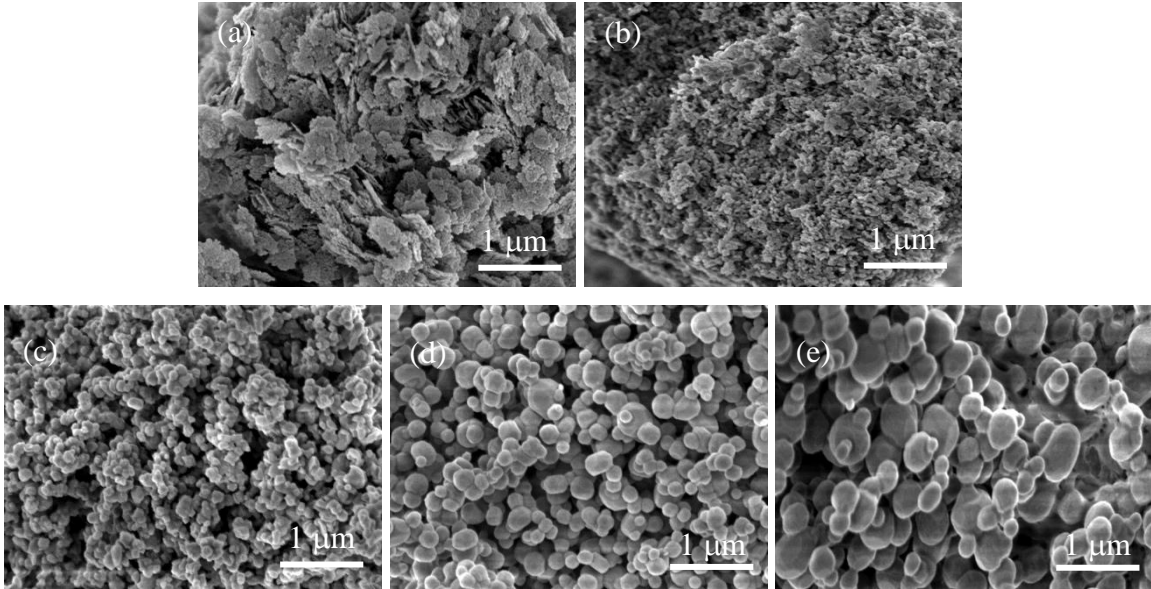


Figure 7 FESEM images of MgO obtained from the calcination of Mg(OH)<sub>2</sub> that was synthesized via the reaction of reject brine with NH<sub>4</sub>OH under (a) 500°C-2h, (b) 600°C-2h, (c) 700°C-2h, (d) 700°C-6h and (e) 700°C-12h

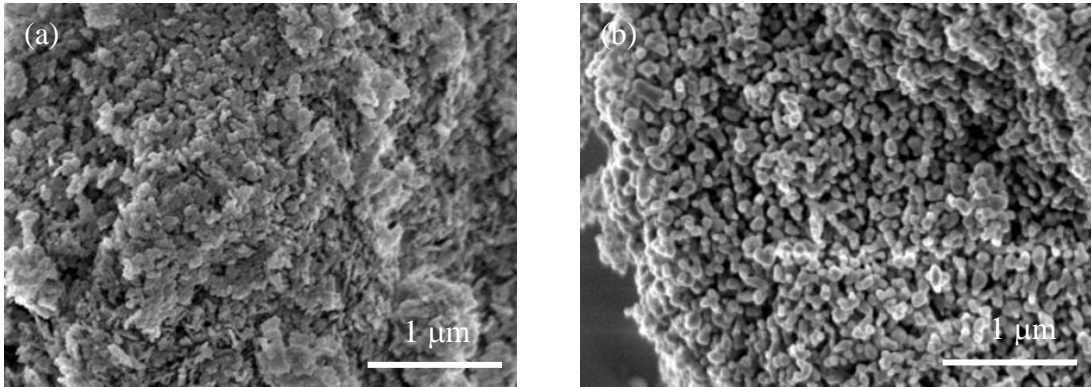


Figure 8 FESEM images of MgO obtained from the calcination of Mg(OH)<sub>2</sub> that was synthesized via the reaction of reject brine with NaOH under (a) 500°C-2h and (b) 700°C-12h (Dong et al., 2018)

### 3.3 Environmental impacts

The industrial production process of reactive MgO from seawater/brine involves four main stages (i) extraction and pre-treatment of seawater/brine (1.30 GJ/tonne MgO); (ii)

1  
2  
3  
4 the preparation of a strong base to be added into seawater/brine (e.g. calcined limestone  
5 (CaO) at an energy consumption of 6.61 GJ/tonne MgO); (iii) the precipitation of  
6 Mg(OH)<sub>2</sub> (exothermic), and (iv) pyro-processing/calcination (8.18 GJ/tonne MgO)  
7 (Hassan, 2013). As a result, the overall energy consumption associated with the  
8 production of reactive MgO from seawater/brine is mainly influenced by the preparation  
9 of the base and the calcination of Mg(OH)<sub>2</sub> during the production of MgO in the final  
10 step. The overall process results in a total energy demand of 16.09 GJ/tonne MgO.  
11 Similarly, the energy consumption of the production of reactive MgO from reject brine  
12 via the addition of NaOH or NH<sub>4</sub>OH is mainly controlled by the production of base  
13 materials (NaOH or NH<sub>4</sub>OH) and the calcination of the obtained Mg(OH)<sub>2</sub> into MgO, as  
14 explained in an earlier study (Dong et al., 2018).  
15  
16  
17  
18  
19  
20  
21  
22  
23  
24  
25

26 As reject brine is a waste generated at the end of the desalination process, the energy  
27 consumption due to the production of reject brine is assumed to be zero. The energy  
28 consumption for the production of 1 tonne of NaOH and NH<sub>3</sub> is around 7.3-9.5 and 27.6-  
29 42.0 GJ, respectively (Fraunhofer, 2009). The energy required for the calcination of  
30 Mg(OH)<sub>2</sub> obtained from reject brine via the addition of NaOH or NH<sub>4</sub>OH for the  
31 production of 1 tonne of reactive MgO was reported to be 6.9 GJ (Dong et al., 2018).  
32 Therefore, the production of 1 tonne of NH<sub>4</sub>OH-based MgO is calculated to be 34.5-48.6  
33 GJ, whereas the production of 1 tonne of NaOH-based MgO can go down to 14.2-16.4 GJ.  
34 While these values are still higher than the energy outputs associated with the production  
35 of MgO via the dry-route (i.e. 5.9 GJ/tonne) (Hassan, 2013), they can be brought down  
36 with the scaling up of the production process and the further optimization of the reaction  
37 paths. Furthermore, the production of MgO via reject brine enables the use of this  
38 harmful waste material, which would otherwise be discharged back into the oceans, and  
39 results in the production of MgO with a higher purity than those typically obtained via  
40 the dry-route.  
41  
42  
43  
44  
45  
46  
47  
48  
49  
50  
51  
52

#### 53 54 55 56 57 **4. Conclusions** 58 59 60 61 62 63 64 65

1  
2  
3  
4 This study presented a comprehensive investigation on the properties of MgO produced  
5 through the calcination of Mg(OH)<sub>2</sub> that was synthesized from reject brine obtained from  
6 a local desalination plant. The influence of two different alkali sources, NH<sub>4</sub>OH and  
7 NaOH, that were used in the synthesis of Mg(OH)<sub>2</sub>, on the properties of Mg(OH)<sub>2</sub> and  
8 MgO was reported. The calcination conditions used during the production of MgO were  
9 varied between 500-700 °C (temperature) and 2-12 hours (residence time) to assess their  
10 effects on the key textural properties, as well as the composition, reactivity and  
11 morphology of MgO.  
12  
13  
14  
15  
16  
17  
18  
19  
20

21 Type of the alkali source used during the synthesis of Mg(OH)<sub>2</sub> had a notable influence  
22 on not only the properties of Mg(OH)<sub>2</sub>, but also on the textural properties, reactivity and  
23 microstructure of MgO. The use of NH<sub>4</sub>OH generated MgO samples with porous  
24 structures, which enabled higher SSA and reactivities than those observed in NaOH-  
25 based samples calcined under the same conditions. The SSA and reactivity of NH<sub>4</sub>OH-  
26 based MgO were more vulnerable to the changes in the calcination conditions and  
27 therefore indicated a sharper decline at higher calcination temperatures and durations,  
28 which was associated with its relatively more porous structure in comparison to NaOH-  
29 based MgO. Out of all the samples studied, NH<sub>4</sub>OH-based Mg(OH)<sub>2</sub> calcined at 500 °C  
30 for 2 hours resulted in the most reactive MgO samples, which possessed the highest SSA  
31 of 78.8 m<sup>2</sup>/g. In terms of its environmental applications, the production of MgO through  
32 these routes required higher amounts of energy than those associated with the production  
33 of MgO via the dry-route. However, improvements are possible via the scaling up of the  
34 production process and the further optimization of the reaction paths.  
35  
36  
37  
38  
39  
40  
41  
42  
43  
44  
45  
46  
47

48 Overall, the obtained results clearly indicated the feasibility of using reject brine as a  
49 reliable source for the recovery of MgO, whose properties and therefore suitability in  
50 various applications, are based on the production conditions (i.e. calcination temperature  
51 and duration) as well as the materials (i.e. alkali source) used during this process. The  
52 characterisation of reactive MgO and the determination of the relationship between the  
53 production conditions and performance of the final product revealed in this paper will  
54 enable the end users to determine the most suitable application in line with the properties  
55  
56  
57  
58  
59  
60  
61  
62  
63  
64  
65

1  
2  
3  
4 of the MgO obtained. MgO with a high reactivity (i.e. SSA over 60 m<sup>2</sup>/g) is categorized  
5 as highly reactive (Jin and Al-Tabbaa, 2014), which could be used as a fertiliser,  
6 chemical absorbent or in filtration mediums (Lee et al., 2004; Moussavi and Mahmoudi,  
7 2009b; Pilarska et al., 2017; Shand, 2006). On the other hand, MgO with a medium  
8 reactivity (i.e. SSA over 10 m<sup>2</sup>/g) could be used in the construction industry as a binder  
9 or an additive, depending on the mix design and project requirements (Shand, 2006).  
10  
11  
12  
13  
14  
15  
16  
17  
18

### 19 **Acknowledgements**

20  
21  
22 This project is funded by the National Research Foundation (NRF), Prime Minister's  
23 Office, Singapore under its Campus for Research Excellence and Technological  
24 Enterprise (CREATE) program.  
25  
26  
27  
28  
29  
30  
31

### 32 **References**

- 33  
34  
35 Al-Tabbaa, A., 2013. Reactive magnesia cement. In: F. PachecoTorgal, S. Jalali, J.  
36 Labrincha and V.M. John (Eds.), *Eco-Efficient Concrete*. Woodhead Publishing Series in  
37 Civil and Structural Engineering, pp. 523-543.  
38  
39 Alvarado, E., Torres-Martinez, L.M., Fuentes, A.F. and Quintana, P., 2000. Preparation  
40 and characterization of MgO powders obtained from different magnesium salts and the  
41 mineral dolomite. *Polyhedron*, 19(22-23): 2345-2351.  
42  
43 Bartley, J.K. et al., 2012. Simple method to synthesize high surface area magnesium  
44 oxide and its use as a heterogeneous base catalyst. *Applied Catalysis B-Environmental*,  
45 128: 31-38.  
46  
47 Boyd, C.E., 2015. *Water Quality: An Introduction*. Springer International Publishing.  
48  
49 Boynton, R.S., 1980. *Chemistry and technology of lime and limestone*. John wiley.  
50  
51 Caraballo, M.A., Rotting, T.S., Macias, F., Nieto, J.M. and Ayora, C., 2009. Field multi-  
52 step limestone and MgO passive system to treat acid mine drainage with high metal  
53 concentrations. *Applied Geochemistry*, 24(12): 2301-2311.  
54  
55  
56  
57  
58  
59  
60  
61  
62  
63  
64  
65

1  
2  
3  
4 Choudhary, V.R., Rane, V.H. and Gadre, R.V., 1994. Influence of Precursors Used in  
5 Preparation of MgO on Its Surface Properties and Catalytic Activity in Oxidative  
6 Coupling of Methane. *Journal of Catalysis*, 145(2): 300-311.  
7  
8  
9  
10 Dave, R.H. and Ghosh, P.K., 2005. Enrichment of bromine in sea-bittern with recovery  
11 of other marine chemicals. *Industrial & Engineering Chemistry Research*, 44(9): 2903-  
12 2907.  
13  
14  
15 Ding, Y. et al., 2001. Nanoscale magnesium hydroxide and magnesium oxide powders:  
16 control over size, shape, and structure via hydrothermal synthesis. *Chemistry of Materials*,  
17 13(2): 435-440.  
18  
19  
20  
21 Dong, H.L., Unluer, C., Yang, E.H. and Al-Tabbaa, A., 2017. Synthesis of reactive MgO  
22 from reject brine via the addition of NH<sub>4</sub>OH. *Hydrometallurgy*, 169: 165-172.  
23  
24  
25 Dong, H.L., Unluer, C., Yang, E.H. and Al-Tabbaa, A., 2018. Recovery of reactive MgO  
26 from reject brine via the addition of NaOH. *Desalination*, 429: 88-95.  
27  
28  
29  
30  
31  
32  
33  
34  
35  
36  
37  
38  
39  
40  
41  
42  
43  
44  
45  
46  
47  
48  
49  
50  
51  
52  
53  
54  
55  
56  
57  
58  
59  
60  
61  
62  
63  
64  
65

Dung, N. and Unluer, C., 2017a. Carbonated MgO concrete with improved performance:  
The influence of temperature and hydration agent on hydration, carbonation and strength  
gain. *Cement and Concrete Composites*.

Dung, N. and Unluer, C., 2017b. Sequestration of CO<sub>2</sub> in reactive MgO cement-based  
mixes with enhanced hydration mechanisms. *Construction and Building Materials*, 143:  
71-82.

El-Naas, M.H., 2011. *Reject brine management*. INTECH Open Access Publisher.

Eubank, W.R., 1951. Calcination studies of magnesium oxides. *Journal of the American  
Ceramic Society*, 34(8): 225-229.

Fan, W. et al., 2004. Controlled synthesis of single-crystalline Mg (OH)<sub>2</sub> nanotubes and  
nanorods via a solvothermal process. *Journal of Solid State Chemistry*, 177(7): 2329-  
2338.

Fraunhofer, E., 2009. Developing Benchmarking Criteria for CO<sub>2</sub> Emissions. In: E.D.-G.  
European Commission, Service contract (Ed.).

Gao, P. et al., 2008. Production of MgO-type expansive agent in dam concrete by use of  
industrial by-products. *Building and Environment*, 43(4): 453-457.

Hanlon, J.M. et al., 2015. Rapid surfactant-free synthesis of Mg(OH)<sub>2</sub> nanoplates and  
pseudomorphic dehydration to MgO. *Crystengcomm*, 17(30): 5672-5679.

1  
2  
3  
4 Harrison, A.J.W., 2008. Reactive magnesium oxide cements.  
5  
6 Hassan, D., 2013. Environmental Sustainability Assessment & Associated Experimental  
7  
8 Investigations of Magnesia Production Routes, University of Cambridge.  
9  
10 Henrist, C., Mathieu, J.-P., Vogels, C., Rulmont, A. and Cloots, R., 2003. Morphological  
11  
12 study of magnesium hydroxide nanoparticles precipitated in dilute aqueous solution.  
13  
14 Journal of Crystal Growth, 249(1): 321-330.  
15  
16 Itatani, K., Itoh, A., Howell, F.S., Kishioka, A. and Kinoshita, M., 1993. Densification  
17  
18 and microstructure development during the sintering of submicrometer magnesium-oxide  
19  
20 particles prepared by a vapor-phase oxidation process. Journal of Materials Science,  
21  
22 28(3): 719-728.  
23  
24 Itatani, K., Koizumi, K., Howell, F.S., Kishioka, A. and Kinoshita, M., 1988.  
25  
26 Agglomeration of magnesium oxide particles formed by the decomposition of  
27  
28 magnesium hydroxide .1. Agglomeration at increasing temperature. Journal of Materials  
29  
30 Science, 23(9): 3405-3412.  
31  
32 Itatani, K., Nomura, M., Kishioka, A. and Kinoshita, M., 1986. Sinterability of various  
33  
34 high-purity magnesium-oxide powders. Journal of Materials Science, 21(4): 1429-1435.  
35  
36 Jin, F. and Al-Tabbaa, A., 2014. Characterisation of different commercial reactive  
37  
38 magnesia. Advances in Cement Research, 26(2): 101-113.  
39  
40 Khuyen Thi, T., Han, K.S., Kim, S.J., Kim, M.J. and Tam, T., 2016. Recovery of  
41  
42 magnesium from Uyuni salar brine as hydrated magnesium carbonate. Hydrometallurgy,  
43  
44 160: 106-114.  
45  
46 Knibbs, N.V.S., 1924. Lime and magnesia.  
47  
48 Kontoyannis, C.G. and Vagenas, N.V., 2000. Calcium carbonate phase analysis using  
49  
50 XRD and FT-Raman spectroscopy. The Analyst, 125(2): 251-255.  
51  
52 Lee, E.K., Jung, K.D., Joo, O.S. and Shul, Y.G., 2004. Magnesium oxide as an effective  
53  
54 catalyst in catalytic wet oxidation of H<sub>2</sub>S to sulfur. Reaction Kinetics and Catalysis  
55  
56 Letters, 82(2): 241-246.  
57  
58 Liska, M., Al-Tabbaa, A., Carter, K. and Fifield, J., 2012a. Scaled-up commercial  
59  
60 production of reactive magnesium cement pressed masonry units. Part I: Production.  
61  
62 Proceedings of the Institution of Civil Engineers-Construction Materials, 165(4): 211-223.  
63  
64  
65



1  
2  
3  
4 Liska, M., Al-Tabbaa, A., Carter, K. and Fifield, J., 2012b. Scaled-up commercial  
5 production of reactive magnesia cement pressed masonry units. Part II: Performance.  
6 Proceedings of the Institution of Civil Engineers-Construction Materials, 165(4): 225-243.  
7  
8 Markov, I.V., 2016. Crystal Growth for Beginners: Fundamentals of Nucleation, Crystal  
9 Growth and Epitaxy. World Scientific Publishing Company.  
10  
11 Mo, L.W., Deng, M. and Tang, M.S., 2010. Effects of calcination condition on expansion  
12 property of MgO-type expansive agent used in cement-based materials. Cement and  
13 Concrete Research, 40(3): 437-446.  
14  
15 Mo, L.W., Deng, M., Tang, M.S. and Al-Tabbaa, A., 2014. MgO expansive cement and  
16 concrete in China: Past, present and future. Cement and Concrete Research, 57: 1-12.  
17  
18 Moussavi, G. and Mahmoudi, M., 2009a. Removal of azo and anthraquinone reactive  
19 dyes from industrial wastewaters using MgO nanoparticles. Journal of Hazardous  
20 Materials, 168(2-3): 806-812.  
21  
22 Moussavi, G. and Mahmoudi, M., 2009b. Removal of azo and anthraquinone reactive  
23 dyes from industrial wastewaters using MgO nanoparticles. Journal of Hazardous  
24 Materials, 168(2): 806-812.  
25  
26 Patterson, A.L., 1939. The Scherrer Formula for X-Ray Particle Size Determination.  
27 Physical Review, 56(10): 978-982.  
28  
29 Pilarska, A.A., Klapiszewski, Ł. and Jesionowski, T., 2017. Recent developments in the  
30 synthesis, modification and application of Mg (OH) 2 and MgO: A review. Powder  
31 Technology.  
32  
33 Ruan, S. and Unluer, C., 2016. Comparative life cycle assessment of reactive MgO and  
34 Portland cement production. Journal of Cleaner Production, 137: 258-273.  
35  
36 Shand, M.A., 2006. The Chemistry and Technology of Magnesia. Wiley.  
37  
38 Tran, K.T. et al., 2013. Recovery of magnesium from Uyuni salar brine as high purity  
39 magnesium oxalate. Hydrometallurgy, 138: 93-99.  
40  
41 Turek, M. and Gnot, W., 1995. Precipitation of magnesium hydroxide from brine.  
42 Industrial & Engineering Chemistry Research, 34(1): 244-250.  
43  
44 Unluer, C. and Al-Tabbaa, A., 2013. Impact of hydrated magnesium carbonate additives  
45 on the carbonation of reactive MgO cements. Cement and Concrete Research, 54: 87-97.  
46  
47  
48  
49  
50  
51  
52  
53  
54  
55  
56  
57  
58  
59  
60  
61  
62  
63  
64  
65

1  
2  
3  
4  
5  
6  
7  
8  
9  
10  
11  
12  
13  
14  
15  
16  
17  
18  
19  
20  
21  
22  
23  
24  
25  
26  
27  
28  
29  
30  
31  
32  
33  
34  
35  
36  
37  
38  
39  
40  
41  
42  
43  
44  
45  
46  
47  
48  
49  
50  
51  
52  
53  
54  
55  
56  
57  
58  
59  
60  
61  
62  
63  
64  
65

Unluer, C. and Al-Tabbaa, A., 2014. Enhancing the carbonation of MgO cement porous blocks through improved curing conditions. *Cement and Concrete Research*, 59: 55-65.

Wang, F., Jin, F., Shen, Z.T. and Al-Tabbaa, A., 2016. Three-year performance of in-situ mass stabilised contaminated site soils using MgO-bearing binders. *Journal of Hazardous Materials*, 318: 302-307.

Wright, J.M. and Colling, A., 1995. *Seawater: Its Composition, Properties and Behaviour*. Elsevier Science.

Wu, H., Shao, M., Gu, J. and Wei, X., 2004. Microwave-assisted synthesis of fibre-like Mg (OH) 2 nanoparticles in aqueous solution at room temperature. *Materials Letters*, 58(16): 2166-2169.

Yan, C., Xue, D., Zou, L., Yan, X. and Wang, W., 2005. Preparation of magnesium hydroxide nanoflowers. *Journal of Crystal Growth*, 282(3): 448-454.

Word count: 5891

## Investigation of the properties of MgO recovered from reject brine obtained from desalination plants

Haoliang Dong<sup>a</sup>, En-Hua Yang<sup>a</sup>, Cise Unluer<sup>a,\*</sup>, Fei Jin<sup>b</sup>, Abir Al-Tabbaa<sup>c</sup>

<sup>a</sup> School of Civil and Environmental Engineering, Nanyang Technological University, 50 Nanyang Avenue, Singapore 639798, Singapore

<sup>b</sup> School of Engineering, University of Glasgow, Glasgow G12 8QQ, United Kingdom

<sup>c</sup> Department of Engineering, University of Cambridge, Trumpington Street, Cambridge CB2 1PZ, United Kingdom

### Abstract

In addition to its use in various applications such as those in the agriculture, pharmaceutical and refractory industries, MgO is being investigated as a cement binder due to the low calcination temperatures used during its production and its ability to gain strength by absorbing CO<sub>2</sub> in construction products. Similar to the dry-route, the reactivity of MgO synthesised from waste water or reject brine via the calcination of the precipitated Mg(OH)<sub>2</sub> depends on the calcination conditions. This study investigated the influence of two bases, namely ammonia solution (NH<sub>4</sub>OH) and sodium hydroxide (NaOH), on the properties of Mg(OH)<sub>2</sub> precipitated and consequently the characteristics of MgO produced under different calcination conditions. **The energy consumption of the production of reactive MgO from reject brine via the addition of NH<sub>4</sub>OH and NaOH was also reported and compared with the industrial production routes to assess the sustainability of the production procedure.** The final products were characterised in terms of their specific surface area (SSA) and microstructure. Results indicated that Mg(OH)<sub>2</sub> synthesised via the addition of NH<sub>4</sub>OH into reject brine generated a more porous, flake-like morphology than those obtained via the use of NaOH. The SSA and reactivity of NH<sub>4</sub>OH-based MgO demonstrated a sharper decrease with increasing temperature and duration compared to NaOH-based MgO. Out of all samples, NH<sub>4</sub>OH-based MgO calcined at 500 °C for 2 hours revealed the highest reactivity (SSA of 78.8 m<sup>2</sup>/g), which was higher than NaOH-based MgO (SSA of 51.4 m<sup>2</sup>/g).

**Keywords:** *Reject brine; MgO; cement; characterisation; reactivity*

---

\* Corresponding author. Address: N1-01c-74, 50 Nanyang Avenue, Singapore 639798. E-mail address: ucise@ntu.edu.sg (C. Unluer)

## 1. Introduction

Magnesia (MgO) is an important material, which finds various uses in different applications within the refractory, agricultural, pharmaceutical, chemical and construction industries (Caraballo et al., 2009; Lee et al., 2004; Moussavi and Mahmoudi, 2009a; Pilarska et al., 2017; Shand, 2006; Wang et al., 2016). The main production route for MgO involves the calcination of magnesite (i.e. dry-route), as shown in Equation 1. The second method is based on its synthesis from magnesium-rich sources such as seawater or brine (i.e. wet-route), as shown in Equations 2-4.



The calcination conditions used during the production of MgO play a critical role as they determine the properties of the final product. Reactive MgO, produced at 700-1000 °C, through the dry-route, and at lower temperatures of around 500-700 °C through the wet-route, has a high specific surface area (SSA) and maintains a high level of reactivity. Increasing the calcination temperature any further reduces the SSA and reactivity of MgO. Unlike reactive MgO, hard- and dead-burned MgO are produced at > 1000 °C through the dry-route, thereby possessing relatively low SSA and reactivities. Within the construction industry, these MgO types are typically used in applications that exploit their expansive nature (e.g. as expansive agents in mass construction) (Gao et al., 2008; Mo et al., 2014) since their hydration rate is lower than those of reactive MgO or Portland cement (PC). Alternatively, the use of reactive MgO in cement-based formulations does not create any potential late expansion problems due to its similar hydration rate to PC (Dung and Unluer, 2017a; Dung and Unluer, 2017b).

In addition to the lower calcination temperatures used during their production (i.e. 700-1000 °C vs. 1450 °C for PC), reactive MgO-based binders are known to gain strength via carbonation, thereby enabling the permanent sequestration of carbon dioxide (CO<sub>2</sub>) within a range of construction products (Al-Tabbaa, 2013; Harrison, 2008; Liska et al., 2012a; Liska et al., 2012b; Unluer and Al-Tabbaa, 2013; Unluer and Al-Tabbaa, 2014).

The strength gain mechanism of reactive MgO within cement-based applications involves its hydration to form  $\text{Mg}(\text{OH})_2$ , which then carbonates into a range of strength providing carbonate phases. During this process, the rate and the degree of these reactions, and hence strength gain, are controlled by many factors. One of the key factors influencing the strength and microstructural development of reactive MgO-based formulations is the reactivity of MgO, which is determined via its production parameters (Ruan and Unluer, 2016).

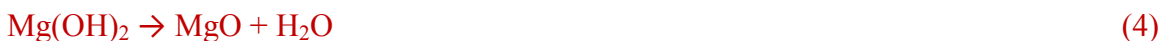
Other than magnesite and other Mg-bearing minerals which serve as a source for MgO through the dry-route, seawater contains an average  $\text{Mg}^{2+}$  concentration of 1.29-1.35 g/L, thereby constituting a significant resource of magnesium (Boyd, 2015; Wright and Colling, 1995). Unlike the dry-route, the wet-route involves the precipitation of  $\text{Mg}(\text{OH})_2$  from the brine solution, which is then calcined to produce MgO. The characteristics of  $\text{Mg}(\text{OH})_2$ , such as its crystal size, shape and structure are strongly influenced by the type of solvent and base used during its production, and the pH and temperature of reaction, at the end of which  $\text{Mg}(\text{OH})_2$  with different morphologies (i.e. rod-, tube-, needle- and lamella-like etc.) can be obtained (Alvarado et al., 2000; Ding et al., 2001; Fan et al., 2004; Henrist et al., 2003; Wu et al., 2004; Yan et al., 2005).

Depending on the equilibrium constant values and dissociation degrees, a base, which releases  $\text{OH}^-$  ions in an aqueous solution, can be categorized as a strong or weak base. An example to these base materials, sodium hydroxide (NaOH), introduced as an alkali source into  $\text{MgCl}_2$  solutions, was found to produce  $\text{Mg}(\text{OH})_2$  with a globular, cauliflower-like morphology. Alternatively, the use of another base, ammonia ( $\text{NH}_4\text{OH}$ ), resulted in  $\text{Mg}(\text{OH})_2$  with a plate-like morphology, which was associated with the differences in the type of base and pH of the solution (Henrist et al., 2003). As the isoelectric point (IEP) of  $\text{Mg}(\text{OH})_2$  is situated at  $\sim 12$ , the higher pH induced by the addition of NaOH causes the surface to be negatively charged, where  $\text{Na}^+$  derived from NaOH can easily be adsorbed without any selectivity. This mechanism hinders the attachment of  $\text{Mg}^{2+}$  to the surface, resulting in its isotropic growth and aggregation that leads to the formation of a globular cauliflower-like morphology. By contrast, the

positively charged surface of particles due to the lower pH and IEP induced by  $\text{NH}_4\text{OH}$  favours the adsorption of  $\text{Mg}^{2+}$ . Furthermore, the larger size of  $\text{NH}_4^+$  than  $\text{Na}^+$ , which is not easily adsorbed on the crystal facets, results in the anisotropic growth of particles and thus the formation of a plate-like morphology.

Reject brine, a concentrated by-product obtained from treating brackish water or seawater in desalination plants, has a great potential to be used as an MgO source due to its high  $\text{Mg}^{2+}$  content (i.e. 30% more than seawater) and abundance on both local and global levels. It is estimated that the world production of desalination water exceeds 30 million  $\text{m}^3/\text{day}$ , which generates an equivalent amount of reject brine (El-Naas, 2011). The highly saline effluent brine from the desalination process not only has no economic value, but also has adverse effects on the marine ecosystem as it is currently discharged back into the sea. This process disturbs the local water and sediment by introducing a multi-component waste and increasing the temperature, also endangering the marine organisms due to the residual chemicals mixed into the brine from the pre-treatment process. Production of MgO from reject brine provides a new purpose for this otherwise harmful waste material and proposes a potentially sustainable alternative for the current production of MgO.

The extraction of MgO from reject brine involves the use of a base, such as slaked lime ( $\text{Ca}(\text{OH})_2$ ), dolime ( $\text{CaO}\cdot\text{MgO}$ ), NaOH or  $\text{NH}_4\text{OH}$  to enable the precipitation of  $\text{Mg}(\text{OH})_2$  in the first stage (Dave and Ghosh, 2005; Khuyen Thi et al., 2016; Tran et al., 2013; Turek and Gnot, 1995). The obtained  $\text{Mg}(\text{OH})_2$  is then heated to around 400-500 °C, leading to the production of MgO, as illustrated in Equations 2-4.



The parameters that influence the properties of MgO obtained via the calcination of  $\text{MgCO}_3$  or  $\text{Mg}(\text{OH})_2$  have been reported by several studies (Alvarado et al., 2000; Bartley

et al., 2012; Choudhary et al., 1994; Eubank, 1951; Itatani et al., 1988; Mo et al., 2010). The main parameters that control the properties of the final product have been identified as calcination conditions (i.e. temperature and duration), as well as the characteristics of the precursor (i.e. physical properties and chemical composition). Accordingly, the decomposition temperature of  $\text{MgCO}_3$  is between 400 and 750 °C, which depends on its impurity level, crystallographic structure, microstructure and production conditions (Boynton, 1980; Knibbs, 1924; Shand, 2006). Increasing the calcination temperature and duration decreases the SSA and hence the reactivity of MgO (Mo et al., 2010), thereby controlling its performance in various applications.

The feasibility of producing MgO with a high reactivity from reject brine via the addition of  $\text{NH}_4\text{OH}$  and  $\text{NaOH}$  has been presented in previous studies (Dong et al., 2017; Dong et al., 2018). One of the main factors determining the efficiency of the overall synthesis was the type and amount of the base introduced into the reject brine. Accordingly, the characteristics of  $\text{Mg}(\text{OH})_2$  and resulting MgO significantly varied under the use of different bases, especially in terms of reactivity and microstructure. However, the influence of base type, and reaction and calcination conditions on the textural properties (i.e. SSA and pore size distribution) and reactivity of the MgO obtained from reject brine has not been revealed yet.

For the accurate characterization of the final product, the relationship between these key parameters (i.e. base type and reaction/calcination conditions) on the properties of MgO must be thoroughly comprehended. Establishing clear links between the production conditions and final properties of MgO will enable its effective use and the identification of the right applications in line with its capabilities. With this goal in mind, this paper presents a comprehensive characterization of MgO obtained via the calcination of  $\text{Mg}(\text{OH})_2$  precipitated using two different bases ( $\text{NH}_4\text{OH}$  and  $\text{NaOH}$ ) and compares the properties of the final product produced under different calcination conditions. The obtained results shed a light on the influence of different base environments and calcination conditions on the properties of MgO and highlighted potential application areas that can benefit from the end product. **The energy consumption of the production of**

reactive MgO from reject brine via the addition of NaOH and NH<sub>4</sub>OH was also reported and compared with the industrial production of MgO from seawater/brine and the dry-route to evaluate the utilization of reject brine from a sustainability standpoint.

## 2. Materials and Methodology

### 2.1. Materials

Reject brine, whose cation composition obtained via inductively coupled plasma-optical emission spectroscopy (ICP-OES) is listed in Table 1, was provided by a local desalination plant in Singapore. Ammonium hydroxide solution (NH<sub>4</sub>OH with 25% NH<sub>3</sub> content) and sodium hydroxide (NaOH), used as the alkaline sources in the synthesis of Mg(OH)<sub>2</sub>, were supplied by Sigma-Aldrich and VWR Pte Ltd in Singapore, respectively.

Table 1 Chemical composition of reject brine used in this study

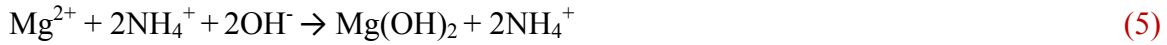
Element/ Concentration	Cl	Na	SO <sub>4</sub>	Mg	K	Ca	Sr	B	Si	Li	P	Al
ppm	65593.	16124.	4322.	1679.	808.	563.	5.	4.	0.	0.	0.	0.
	1	3	6	0	5	6	3	5	5	4	2	1

### 2.2. Methodology

The first step involved the synthesis of Mg(OH)<sub>2</sub> from reject brine via the addition of the bases, in line with the procedure explained in detail in previous studies (Dong et al., 2017; Dong et al., 2018). NH<sub>4</sub>OH was included at a NH<sub>4</sub>OH/Mg<sup>2+</sup> molar ratio of 6, whereas NaOH was added at a NaOH/Mg<sup>2+</sup> molar ratio of 2 to achieve Mg(OH)<sub>2</sub> with the highest purity and yield, as optimized in the aforementioned previous studies. Mg(OH)<sub>2</sub> that precipitated at the end of the reactions shown in Equations 5 and 6 was calcined to



produce MgO. The calcination process involved the heating of Mg(OH)<sub>2</sub> at a rate of 10 °C/min to reach three different calcination temperatures (500, 600 and 700 °C), which were each maintained for three different residence times (2, 6 and 12 hours).



As a detailed analysis and characterization of Mg(OH)<sub>2</sub> obtained via the reaction of reject brine with NH<sub>4</sub>OH and NaOH was presented earlier (Dong et al., 2017; Dong et al., 2018), this study mainly focused on the characterization and comparison of the final product, MgO, obtained via the use of two distinct bases under different calcination conditions. A Bruker D8 Advance with a Cu K $\alpha$  source was used to perform X-ray powder diffraction (XRD) under the operation conditions of 40 kV and 40 mA, emitting radiation with a wavelength of 1.5405 Å, scan rate of 0.02 °/step, and a 2 $\theta$  range of 5 to 70°. The microstructures of the solids were analysed by imaging powder surface via a JSM-7600F thermal field emission scanning electron microscopy (FESEM), **operated under a vacuum condition of 2.5×10<sup>-3</sup> Pa and 2 kV**. The thermo-properties of the final phases were characterized via thermogravimetric and differential thermal analysis (TG/DTA) using a PyrisDiamond TGA 4000 operated at a heating rate of 10 °C/min under air flow. The texture properties, namely SSA and pore volume, were determined from nitrogen adsorption-desorption isotherms using a Quadrasorb Evo automated surface area and pore size analyser. The SSA was calculated by Brunauer-Emmett-Teller (BET) method, while the pore volume was determined by Barrett-Joyner-Halenda (BJH) method. The reactivity of MgO was tested via the measurement of the time required to neutralize an acid solution with a phenolphthalein pH indicator. This acid reactivity test involved the use of 0.28 grams of synthesized MgO, which was added into 50 ml of 0.07 mol/L citric acid solution (Mo et al., 2010; Shand, 2006).

**The agglomeration ratio, defined as  $G_{\text{BET}}/G_{\text{XRD}}$ , involved the calculation of the primary particle size ( $G_{\text{BET}}$ ), which was obtained from the SSA and crystallite size.  $G_{\text{BET}}$  was calculated according to the equation  $G_{\text{BET}} = F/\rho S$ , where F is the particle-shape factor (6),**

S is the SSA ( $\text{m}^2/\text{g}$ ) and  $\rho$  is the theoretical density of MgO ( $3.595 \text{ g/cm}^3$ ) (Itatani et al., 1986). The crystallite size ( $G_{\text{XRD}}$ ) was calculated according to  $G_{\text{XRD}} = K \cdot \lambda / (\beta \cdot \cos(\theta))$ , where  $\lambda$  is the wavelength of Cu K $\alpha$  ( $1.5405 \text{ \AA}$ ),  $\beta$  is the full width at half-maximum intensity (FWHM) of a Bragg reflection subtracting the instrumental broadening,  $\theta$  is the Bragg angle and K is the shape factor with a typical value as 0.9 (Patterson, 1939).

### 3. Results and Discussions

#### 3.1. Characterization of Mg(OH)<sub>2</sub>

##### 3.1.1. Composition and textural properties

Figure 1 shows the XRD diffractograms of the synthesized Mg(OH)<sub>2</sub> obtained via the reaction between reject brine and two different base solutions involving the use of NH<sub>4</sub>OH and NaOH. The two diffraction patterns presented similar phases, which were mainly attributed to Mg(OH)<sub>2</sub>, along with minor amounts of CaCO<sub>3</sub> in the crystal form of aragonite. As discussed in previous studies (Dong et al., 2017; Dong et al., 2018), the elevated molar ratios of NH<sub>4</sub>OH/Mg<sup>2+</sup> and NaOH/Mg<sup>2+</sup> lead to a shift in the crystal structure of CaCO<sub>3</sub> from aragonite to calcite without changing the properties of Mg(OH)<sub>2</sub>. Regardless of the base material used, as the main goal was to determine the optimum ratios that led to the production of Mg(OH)<sub>2</sub> and subsequently MgO with the highest purity and yield via each reaction path, the molar ratios of NH<sub>4</sub>OH/Mg<sup>2+</sup> and NaOH/Mg<sup>2+</sup> were determined as 6 and 2, respectively. Although two different ratios were used for each base material, the composition of Mg(OH)<sub>2</sub> synthesized via the use of these different base solutions did not differ and resulted in a similarly high purity level of ~94% for both cases, as detailed in Table 2, along with other textural properties.

In addition to the purity level, the crystallite size of both samples was calculated according to the Debye-Scherrer formula. The major characteristic peak of Mg(OH)<sub>2</sub> at  $38.1^\circ 2\theta$  was used in this calculation. NH<sub>4</sub>OH- and NaOH-based Mg(OH)<sub>2</sub> possessed a

crystallite size of 15.4 and 10.5 nm, respectively. The differences in the crystallite sizes of both samples could be associated with the different strengths of  $\text{NH}_4\text{OH}$  and  $\text{NaOH}$  as a base and the chemical nature of ions present in the solution.  $\text{NaOH}$ , which is a strong base, ionizes completely and produces a significant number of  $\text{OH}^-$  once dissolved in water. On the other hand,  $\text{NH}_4\text{OH}$  is a weaker base and electrolyte, which only ionizes to a limited extent in water, gradually releasing  $\text{OH}^-$  into the solution. The higher concentration of  $\text{OH}^-$  provided by  $\text{NaOH}$  could accelerate the reaction of  $\text{Mg}^{2+}$  with  $\text{OH}^-$ , thereby enhancing the formation of  $\text{Mg}(\text{OH})_2$  crystals and resulting in a shorter reaction time. The elevated pH value created a high supersaturation level, which formed a larger amount of **particles** and generated a faster nucleation process, and hence smaller crystals (Markov, 2016).

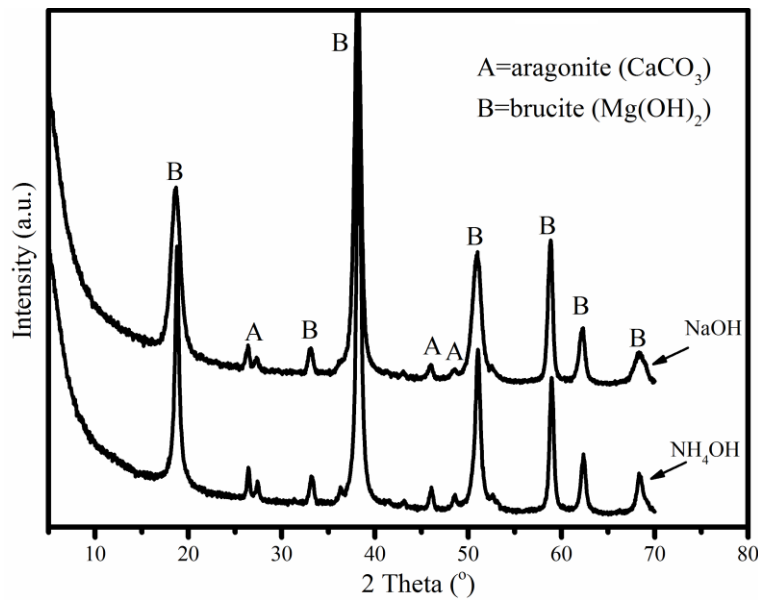


Figure 1 XRD diffractograms of  $\text{Mg}(\text{OH})_2$  obtained from the reaction of reject brine with  $\text{NH}_4\text{OH}$  and  $\text{NaOH}$  (Dong et al., 2017; Dong et al., 2018)

Table 2 Chemical composition, crystallite size, SSA and pore volume of  $\text{Mg}(\text{OH})_2$  obtained from the reaction of reject brine with  $\text{NH}_4\text{OH}$  and  $\text{NaOH}$

Base	Phase contents (%)		$G_{\text{XRD}}$ (nm)	SSA ( $\text{m}^2/\text{g}$ )	Pore volume ( $\text{cm}^3/\text{g}$ )
	$\text{Mg}(\text{OH})_2$	$\text{CaCO}_3$			
$\text{NH}_4\text{OH}$	93.5	6.5	15.4	10.6	0.055

NaOH	93.7	6.3	10.5	7.4	0.029
------	------	-----	------	-----	-------

### 3.1.2. Microstructure

The morphology of  $\text{Mg}(\text{OH})_2$  obtained via the addition of  $\text{NH}_4\text{OH}$  and  $\text{NaOH}$  to reject brine was further investigated through FESEM, as shown in Figure 2. The use of  $\text{NaOH}$  generated a densely packed granular morphology with relatively clear boundaries. Alternatively, those produced via the use of  $\text{NH}_4\text{OH}$  demonstrated a flake-like morphology with a more porous structure, which was in line with the findings of previous studies (Henrist et al., 2003).

These microstructural observations were confirmed by BET results that revealed the SSA of  $\text{Mg}(\text{OH})_2$  produced through these two distinct routes. As shown in Table 2,  $\text{NH}_4\text{OH}$ - and  $\text{NaOH}$ -based  $\text{Mg}(\text{OH})_2$  possessed a SSA of 10.6 and 7.4  $\text{m}^2/\text{g}$ , respectively. Furthermore, the pore volumes of both samples were recorded as 0.055 and 0.029  $\text{cm}^3/\text{g}$ , respectively. This morphological difference could be related to the pH and cations present in each solution (Hanlon et al., 2015; Henrist et al., 2003). The introduction of the strong base,  $\text{NaOH}$ , set the pH of solution beyond the IEP of  $\text{Mg}(\text{OH})_2$  (~12) (Hanlon et al., 2015). Furthermore, the high supersaturation generated by  $\text{NaOH}$  enhanced the nucleation of tiny crystals, which agglomerated together and generated a much denser structure with a lower porosity, therefore resulting in a lower SSA. On the other hand, the addition of the weaker base,  $\text{NH}_4\text{OH}$ , favoured the binding of  $\text{OH}^-$  to the basal plane, leading to anisotropic growth and hence the formation of a flake-like structure.

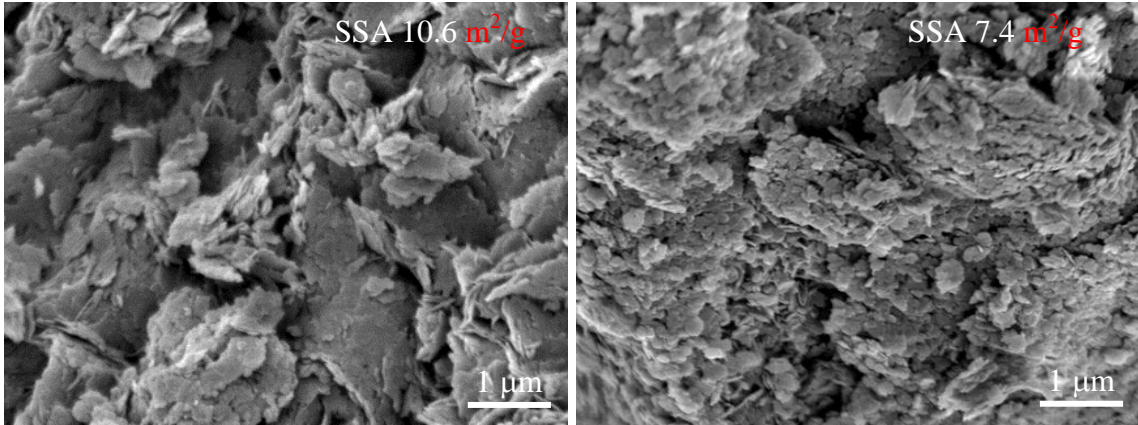


Figure 2 FESEM images of  $\text{Mg}(\text{OH})_2$  obtained from the reaction of reject brine with (a)  $\text{NH}_4\text{OH}$  and (b)  $\text{NaOH}$  (Dong et al., 2017; Dong et al., 2018)

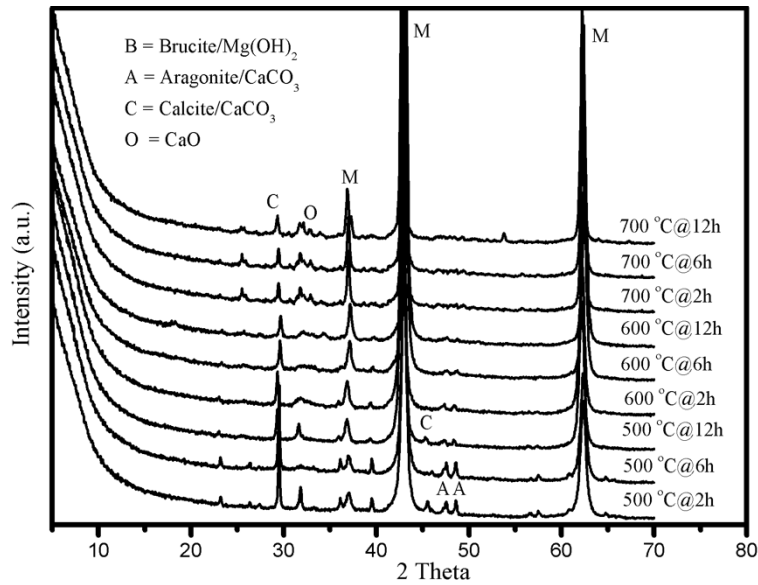
### 3.2. Characterization of MgO

#### 3.2.1. Composition

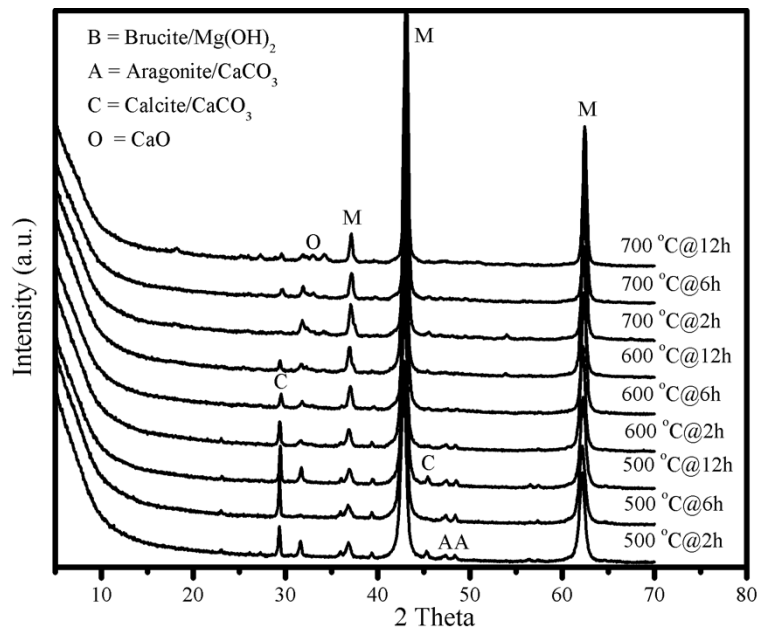
The XRD patterns of MgO, obtained from the calcination of  $\text{Mg}(\text{OH})_2$ , generated via the reaction of reject brine with  $\text{NH}_4\text{OH}$  and  $\text{NaOH}$ , under different calcination conditions are shown in Figures 3(a) and 3(b), respectively. In both cases,  $\text{Mg}(\text{OH})_2$  was completely decomposed into MgO under the calcination conditions studied (i.e. 500-700 °C for 2-12 hours). The characteristic peaks of MgO, which were located at 37.0°, 43.1° and 62.3°  $2\theta$ , matched well with the reference peaks of MgO indicated in JCPDS card no. 89-7746. Along with MgO, a few minor peaks attributed to  $\text{CaCO}_3$  and CaO were observed in the XRD patterns of all samples.

Aragonite (primary peaks at 47.5° and 48.6°  $2\theta$ ), which was initially present within the sample composition, gradually transformed into calcite (primary peaks at 29.5° and 43.1°  $2\theta$ ) at higher calcination temperatures (600 °C). This was because aragonite is known to convert to calcite, which possesses a higher entropy and is more stable, at temperatures above 400 °C (Kontoyannis and Vagenas, 2000). The clear reduction in the intensity of the calcite peak at 29.5°  $2\theta$  indicated the decomposition of  $\text{CaCO}_3$  into CaO as the

calcination temperature further increased to 700 °C. The overall results demonstrated the similar phase transitions of NH<sub>4</sub>OH- and NaOH-based samples under increasing calcination temperatures and durations, which were in line with the findings reported earlier (Dong et al., 2017; Dong et al., 2018). These outcomes highlighted that, albeit their similar compositions, the final products differed in terms of their physical properties and morphology, which were determined by the production parameters.



(a)



(b)

Figure 3 XRD diffractograms of reactive MgO obtained from the calcination of Mg(OH)<sub>2</sub> that was synthesized via the reaction of reject brine with (a) NH<sub>4</sub>OH and (b) NaOH, under different calcination temperatures and durations

### 3.2.2. Textural properties

The SSA values of MgO, obtained from the calcination of Mg(OH)<sub>2</sub> generated via the reaction of reject brine with NH<sub>4</sub>OH and NaOH under different calcination conditions (i.e. temperature and duration), are displayed in Figure 4. **The data on the production of MgO at 500 °C for 2 hours were taken from previous studies (Dong et al., 2017; Dong et al., 2018).** The SSA values ranged between 5.5 and 78.8 m<sup>2</sup>/g, depending on the base used and the calcination conditions. An increase in the calcination temperature and duration led to a consistent reduction in SSA, indicating a decrease in the reactivity of both NH<sub>4</sub>OH- and NaOH-based MgO samples, whose details are listed in Table 3. The calcination of Mg(OH)<sub>2</sub> involved the release of H<sub>2</sub>O from Mg(OH)<sub>2</sub>, resulting in MgO with a porous structure. Increasing the calcination temperature beyond the decomposition point of Mg(OH)<sub>2</sub> led to the sintering of MgO, breaking down the pores in MgO and causing a reduction in its porosity, thereby increasing its crystallite size (Eubank, 1951). These findings were in line with those reported in previous studies (Alvarado et al., 2000; Eubank, 1951; Itatani et al., 1988; Jin and Al-Tabbaa, 2014; Mo et al., 2010), where the direct influence of calcination conditions on the properties of the final product was reported.

Out of all conditions used in this study, the calcination of NH<sub>4</sub>OH-based Mg(OH)<sub>2</sub> under 500 °C for 2 hours generated the highest SSA of 78.8 m<sup>2</sup>/g, while NaOH-based samples led to corresponding SSA values of 51.4 m<sup>2</sup>/g. Compared with NaOH-based MgO, NH<sub>4</sub>OH-based MgO achieved higher SSA values at lower calcination temperatures (500 °C). This could be due to the difference in the textural properties of the precursor, Mg(OH)<sub>2</sub> (i.e. NH<sub>4</sub>OH-based Mg(OH)<sub>2</sub> possessed a higher SSA and porosity than NaOH-based Mg(OH)<sub>2</sub>). Accordingly, the calcination of NH<sub>4</sub>OH-based Mg(OH)<sub>2</sub> generated

MgO samples with a more porous structure and thereby higher SSA values that corresponding NaOH-based samples at lower calcination temperatures, as shown in Figure 4.

This trend reversed as the calcination temperature increased from 500 to 700 °C, indicating a sharp decline in the SSA and porosity of NH<sub>4</sub>OH-based MgO, whereas the SSA of NaOH-based MgO was not affected at the same rate. At the highest calcination temperature of 700 °C, NaOH-based samples revealed higher SSA and porosity values than NH<sub>4</sub>OH-based ones (SSA of 24.8 vs. 10.3 m<sup>2</sup>/g; porosity of 0.160 vs. 0.041 cm<sup>3</sup>/g), which was especially apparent at shorter residence times (2 and 6 hours). When compared to NaOH-based samples, the porous structures of NH<sub>4</sub>OH-based samples demonstrated a larger reduction in SSA associated with the rapid growth of MgO grains. These differences in SSA values could be attributed to the initially highly porous structure of NH<sub>4</sub>OH-based samples, which were more influenced under elevated calcination conditions. These results indicated that the critical temperature for the sintering of NH<sub>4</sub>OH-based Mg(OH)<sub>2</sub> was lower than that of NaOH-based Mg(OH)<sub>2</sub>, which caused the SSA trend to reverse at higher temperature ranges (Eubank, 1951).

Similar to the calculation of the crystallite size of Mg(OH)<sub>2</sub> that was explained earlier, the major characteristic peak of MgO at 43.1° 2θ was used in the determination of its crystallite size ( $G_{XRD}$ ), which ranged between 10 and 25 nm for both NH<sub>4</sub>OH- and NaOH-based samples. The  $G_{BET}$  values for NH<sub>4</sub>OH- and NaOH-based MgO samples were in the range of 20-350 nm, while the agglomeration ratio ( $G_{BET}/G_{XRD}$ ) ranged between 1.7 and 16.3. The lowest agglomeration ratio of 1.7 was revealed by the NH<sub>4</sub>OH-based sample that was obtained under the calcination conditions of 500 °C for 2 hours. In line with their effect on the SSA of MgO, calcination temperature and duration also had a significant influence on the crystallite size and primary size of MgO, which increased with increasing temperature and duration, regardless of the base utilized. This could be due to the spontaneous coagulation of primary particles under high temperatures and durations (Itatani et al., 1993). Compared with NH<sub>4</sub>OH-based samples, NaOH-based



MgO samples generally achieved higher agglomeration ratios, which could explain the differences in their SSA values, as illustrated in Figure 4.

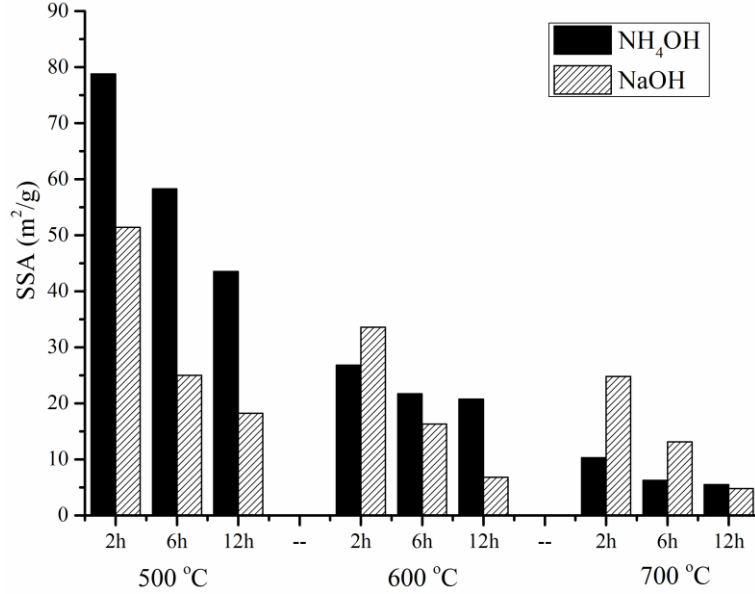


Figure 4 SSA of MgO produced under different calcination temperatures and durations

Table 3 Crystallite size, primary size and pore volume of MgO produced under different calcination temperatures and durations

Base	500 °C			600 °C			700 °C			
	2 h	6 h	12 h	2 h	6 h	12 h	2 h	6 h	12 h	
NH <sub>4</sub> OH	$G_{XRD}$ (nm)	12.6	13.4	14.8	15.5	16.1	17.9	19.5	24.7	24.9
	$G_{BET}$ (nm)	21.2	28.6	38.3	62.3	76.9	80.4	162.0	267.0	303.5
	$G_{BET}/G_{XRD}$	1.7	2.1	2.6	4.0	4.8	4.5	8.3	10.8	12.2
NaOH	Pore volume (cm <sup>3</sup> /g)	0.445	0.371	0.240	0.157	0.117	0.109	0.041	0.029	0.016
	$G_{XRD}$ (nm)	11.4	12.7	13.6	15.0	16.7	18.1	18.9	19.4	21.4
NaOH	$G_{BET}$ (nm)	32.5	66.8	91.7	49.7	102.4	245.4	67.3	127.4	347.7
	$G_{BET}/G_{XRD}$	2.8	5.3	6.8	3.3	6.1	13.6	3.6	6.6	16.3
NaOH	Pore volume (cm <sup>3</sup> /g)	0.317	0.16	0.083	0.166	0.058	0.024	0.160	0.056	0.017

### 3.2.3. Reactivity

Figure 5 shows the acid reactivity of MgO, obtained from the calcination of Mg(OH)<sub>2</sub>, generated via the reaction of reject brine with NH<sub>4</sub>OH and NaOH, under different calcination conditions (Dong et al., 2018). An increase in the neutralization time with an increase in the temperature and duration was observed in all cases, which was an indication of the reduction in reactivity. These findings highlighting the decline in the reaction rate of MgO under elevated calcination conditions were in line with those reported in earlier studies (Jin and Al-Tabbaa, 2014; Mo et al., 2010).

Amongst the two different bases used, NH<sub>4</sub>OH-based MgO samples revealed shorter neutralization times in comparison to NaOH-based ones produced under lower calcination temperatures (500 °C). An increase in the calcination temperature from 500 to 700 °C caused a notable increase in the neutralization times of NH<sub>4</sub>OH-based samples, during which those of NaOH-based samples demonstrated a gradual increase. These trends were in line with the SSA measurements reported earlier in Figure 4, where it was shown that the initially high SSA of NH<sub>4</sub>OH-based samples demonstrated a sharp decrease with increasing calcination temperatures.

The influence of calcination conditions and base type on the properties of MgO was also revealed via a comparison of the SSA and neutralization time (i.e. acid reactivity) of all the samples, as shown in Figure 6 (Dong et al., 2018). The inverse correlation between SSA and neutralization time could be clearly observed in all MgO samples, regardless of the utilized base type. Accordingly, higher SSA values corresponded to shorter neutralization times, which was an indication of the higher reactivity of MgO. Alternatively, lower SSA led to longer neutralization times associated with the lower reactivity and slower reaction of MgO. Although the acid reactivity test could not fully

distinguish amongst MgO samples with high SSA values ( $> 40 \text{ m}^2/\text{g}$ ) as the neutralization time demonstrated by these samples were relatively short, the obtained results clearly indicated the relationship between the two parameters, highlighting the importance of production conditions on the properties of the final product.

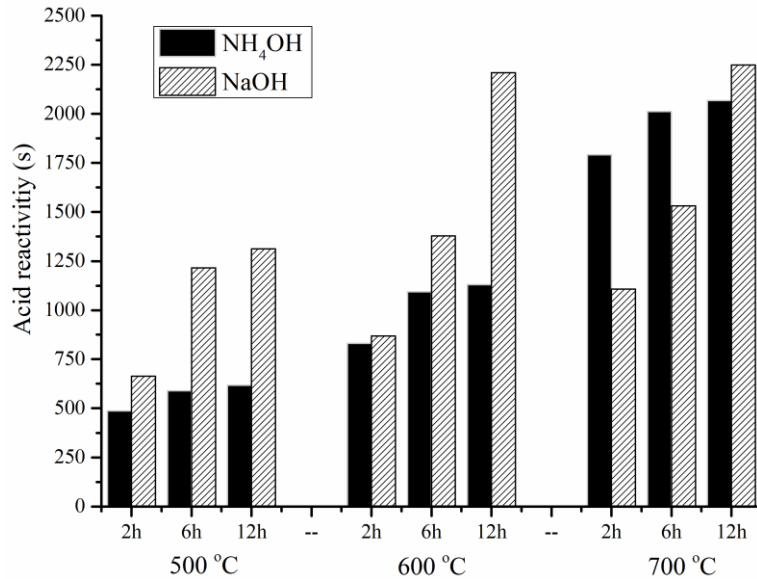


Figure 5 Effect of calcination temperature and duration on the neutralization time of reactive MgO

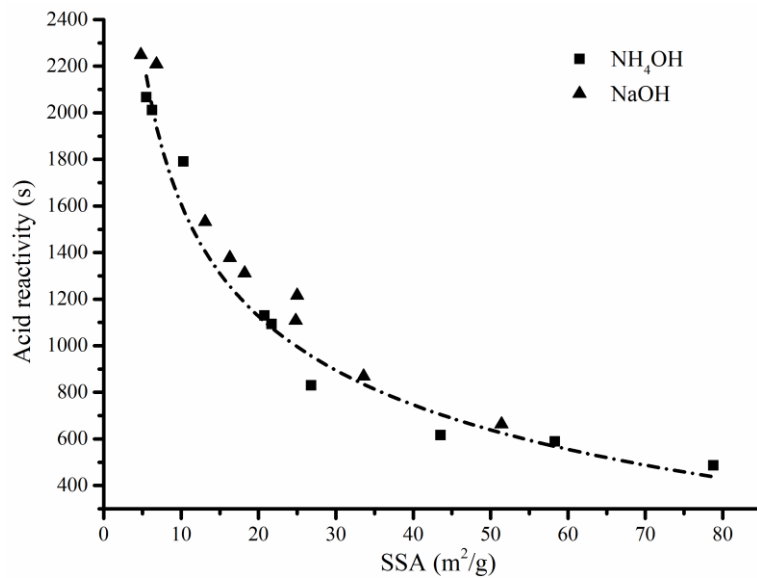


Figure 6 Relationship between the neutralization time (reactivity) and SSA of MgO

### 3.2.4. Microstructure

A further investigation on the influence of the calcination conditions (i.e. temperature and duration) and base type (i.e.  $\text{NH}_4\text{OH}$  and  $\text{NaOH}$ ) on the morphology of the final product ( $\text{MgO}$ ) was revealed through FESEM, as shown in Figures 7 and 8. A single particle of  $\text{MgO}$  consisted of layered grains, which were inherited from the parent material,  $\text{Mg}(\text{OH})_2$ . Increasing the calcination temperature from 500 to 700 °C had a profound effect on the size of the  $\text{MgO}$  grains, resulting in a significant growth in crystallite size, which was accompanied with a reduction in porosity, as seen in Figures 7(a)-(c). The effect of the calcination duration on the morphology of  $\text{MgO}$  was revealed in Figures 7(c)-(e), for which the calcination duration increased from 2 to 12 hours. Production of  $\text{MgO}$  under longer calcination durations led to a noticeable growth in the size of grains. These changes in the morphology of  $\text{MgO}$  grains could clearly explain the reduction of its SSA and the corresponding increase in neutralization time (i.e. decrease of reactivity) under elevated calcination temperatures and durations.

A comparison of Figures 7(a) and 8(a) revealed the porous structure of  $\text{NH}_4\text{OH}$ -based  $\text{MgO}$  in comparison to  $\text{NaOH}$ -based samples, which were both produced under 500 °C for 2 hours. Increasing the calcination temperature and duration to 700 °C for 12 hours led to an increase in the size of  $\text{NH}_4\text{OH}$ -based  $\text{MgO}$  grains, whose growth was much more noticeable than those observed in  $\text{NaOH}$ -based samples ( $G_{\text{XRD}}$  of 24.9 vs. 21.4 nm, listed in Table 3), as demonstrated in Figures 7(e) and 8(b). The increase in the dimensions of the  $\text{MgO}$  grains under high calcination temperatures and durations was attributed to the loss of water during the decomposition of  $\text{Mg}(\text{OH})_2$ , which facilitated the formation of a porous structure. This initial porosity was gradually reduced as the  $\text{MgO}$  grains grew further due to continuous sintering, which was in line with the measurements revealed earlier in Table 3 and findings reported by earlier studies (Mo et al., 2010).

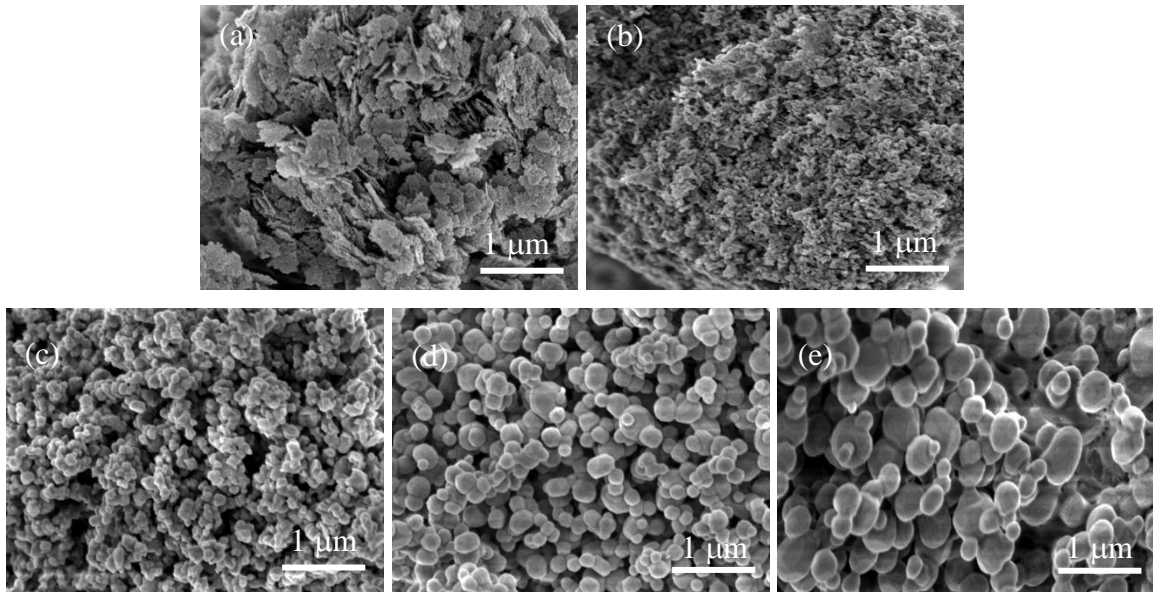


Figure 7 FESEM images of MgO obtained from the calcination of  $\text{Mg}(\text{OH})_2$  that was synthesized via the reaction of reject brine with  $\text{NH}_4\text{OH}$  under (a)  $500^\circ\text{C}$ -2h, (b)  $600^\circ\text{C}$ -2h, (c)  $700^\circ\text{C}$ -2h, (d)  $700^\circ\text{C}$ -6h and (e)  $700^\circ\text{C}$ -12h

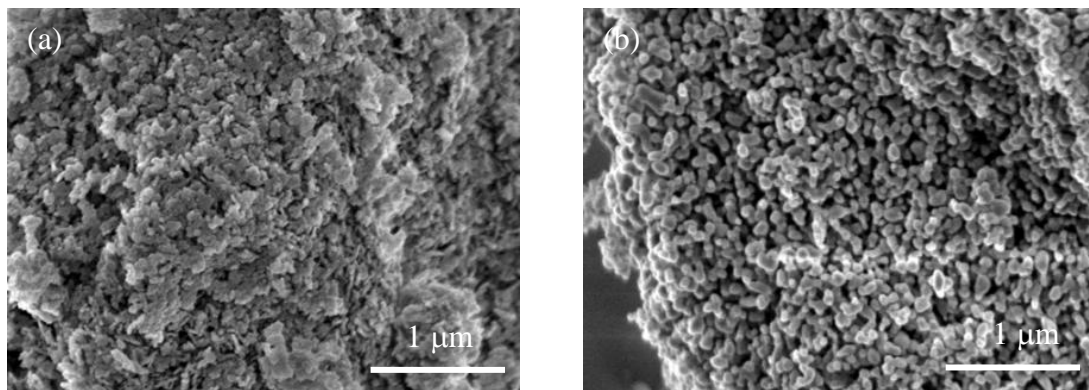


Figure 8 FESEM images of MgO obtained from the calcination of  $\text{Mg}(\text{OH})_2$  that was synthesized via the reaction of reject brine with  $\text{NaOH}$  under (a)  $500^\circ\text{C}$ -2h and (b)  $700^\circ\text{C}$ -12h (Dong et al., 2018)

### 3.3 Environmental impacts

The industrial production process of reactive MgO from seawater/brine involves four main stages (i) extraction and pre-treatment of seawater/brine (1.30 GJ/tonne MgO); (ii)

the preparation of a strong base to be added into seawater/brine (e.g. calcined limestone (CaO) at an energy consumption of 6.61 GJ/tonne MgO); (iii) the precipitation of Mg(OH)<sub>2</sub> (exothermic), and (iv) pyro-processing/calcination (8.18 GJ/tonne MgO) (Hassan, 2013). As a result, the overall energy consumption associated with the production of reactive MgO from seawater/brine is mainly influenced by the preparation of the base and the calcination of Mg(OH)<sub>2</sub> during the production of MgO in the final step. The overall process results in a total energy demand of 16.09 GJ/tonne MgO. Similarly, the energy consumption of the production of reactive MgO from reject brine via the addition of NaOH or NH<sub>4</sub>OH is mainly controlled by the production of base materials (NaOH or NH<sub>4</sub>OH) and the calcination of the obtained Mg(OH)<sub>2</sub> into MgO, as explained in an earlier study (Dong et al., 2018).

As reject brine is a waste generated at the end of the desalination process, the energy consumption due to the production of reject brine is assumed to be zero. The energy consumption for the production of 1 tonne of NaOH and NH<sub>3</sub> is around 7.3-9.5 and 27.6-42.0 GJ, respectively (Fraunhofer, 2009). The energy required for the calcination of Mg(OH)<sub>2</sub> obtained from reject brine via the addition of NaOH or NH<sub>4</sub>OH for the production of 1 tonne of reactive MgO was reported to be 6.9 GJ (Dong et al., 2018). Therefore, the production of 1 tonne of NH<sub>4</sub>OH-based MgO is calculated to be 34.5-48.6 GJ, whereas the production of 1 tonne of NaOH-based MgO can go down to 14.2-16.4 GJ. While these values are still higher than the energy outputs associated with the production of MgO via the dry-route (i.e. 5.9 GJ/tonne) (Hassan, 2013), they can be brought down with the scaling up of the production process and the further optimization of the reaction paths. Furthermore, the production of MgO via reject brine enables the use of this harmful waste material, which would otherwise be discharged back into the oceans, and results in the production of MgO with a higher purity than those typically obtained via the dry-route.

#### **4. Conclusions**

This study presented a comprehensive investigation on the properties of MgO produced through the calcination of Mg(OH)<sub>2</sub> that was synthesized from reject brine obtained from a local desalination plant. The influence of two different alkali sources, NH<sub>4</sub>OH and NaOH, that were used in the synthesis of Mg(OH)<sub>2</sub>, on the properties of Mg(OH)<sub>2</sub> and MgO was reported. The calcination conditions used during the production of MgO were varied between 500-700 °C (temperature) and 2-12 hours (residence time) to assess their effects on the key textural properties, as well as the composition, reactivity and morphology of MgO.

Type of the alkali source used during the synthesis of Mg(OH)<sub>2</sub> had a notable influence on not only the properties of Mg(OH)<sub>2</sub>, but also on the textural properties, reactivity and microstructure of MgO. The use of NH<sub>4</sub>OH generated MgO samples with porous structures, which enabled higher SSA and reactivities than those observed in NaOH-based samples calcined under the same conditions. The SSA and reactivity of NH<sub>4</sub>OH-based MgO were more vulnerable to the changes in the calcination conditions and therefore indicated a sharper decline at higher calcination temperatures and durations, which was associated with its relatively more porous structure in comparison to NaOH-based MgO. Out of all the samples studied, NH<sub>4</sub>OH-based Mg(OH)<sub>2</sub> calcined at 500 °C for 2 hours resulted in the most reactive MgO samples, which possessed the highest SSA of 78.8 m<sup>2</sup>/g. **In terms of its environmental applications, the production of MgO through these routes required higher amounts of energy than those associated with the production of MgO via the dry-route. However, improvements are possible via the scaling up of the production process and the further optimization of the reaction paths.**

Overall, the obtained results clearly indicated the feasibility of using reject brine as a reliable source for the recovery of MgO, whose properties and therefore suitability in various applications, are based on the production conditions (i.e. calcination temperature and duration) as well as the materials (i.e. alkali source) used during this process. **The characterisation of reactive MgO and the determination of the relationship between the production conditions and performance of the final product revealed in this paper will enable the end users to determine the most suitable application in line with the properties**

of the MgO obtained. MgO with a high reactivity (i.e. SSA over 60 m<sup>2</sup>/g) is categorized as highly reactive (Jin and Al-Tabbaa, 2014), which could be used as a fertiliser, chemical absorbent or in filtration mediums (Lee et al., 2004; Moussavi and Mahmoudi, 2009b; Pilarska et al., 2017; Shand, 2006). On the other hand, MgO with a medium reactivity (i.e. SSA over 10 m<sup>2</sup>/g) could be used in the construction industry as a binder or an additive, depending on the mix design and project requirements (Shand, 2006).

### **Acknowledgements**

This project is funded by the National Research Foundation (NRF), Prime Minister's Office, Singapore under its Campus for Research Excellence and Technological Enterprise (CREATE) program.

### **References**

- Al-Tabbaa, A., 2013. Reactive magnesia cement. In: F. PachecoTorgal, S. Jalali, J. Labrincha and V.M. John (Eds.), *Eco-Efficient Concrete*. Woodhead Publishing Series in Civil and Structural Engineering, pp. 523-543.
- Alvarado, E., Torres-Martinez, L.M., Fuentes, A.F. and Quintana, P., 2000. Preparation and characterization of MgO powders obtained from different magnesium salts and the mineral dolomite. *Polyhedron*, 19(22-23): 2345-2351.
- Bartley, J.K. et al., 2012. Simple method to synthesize high surface area magnesium oxide and its use as a heterogeneous base catalyst. *Applied Catalysis B-Environmental*, 128: 31-38.
- Boyd, C.E., 2015. *Water Quality: An Introduction*. Springer International Publishing.
- Boynton, R.S., 1980. *Chemistry and technology of lime and limestone*. John Wiley.
- Caraballo, M.A., Rotting, T.S., Macias, F., Nieto, J.M. and Ayora, C., 2009. Field multi-step limestone and MgO passive system to treat acid mine drainage with high metal concentrations. *Applied Geochemistry*, 24(12): 2301-2311.



Choudhary, V.R., Rane, V.H. and Gadre, R.V., 1994. Influence of Precursors Used in Preparation of MgO on Its Surface Properties and Catalytic Activity in Oxidative Coupling of Methane. *Journal of Catalysis*, 145(2): 300-311.

Dave, R.H. and Ghosh, P.K., 2005. Enrichment of bromine in sea-bittern with recovery of other marine chemicals. *Industrial & Engineering Chemistry Research*, 44(9): 2903-2907.

Ding, Y. et al., 2001. Nanoscale magnesium hydroxide and magnesium oxide powders: control over size, shape, and structure via hydrothermal synthesis. *Chemistry of Materials*, 13(2): 435-440.

Dong, H.L., Unluer, C., Yang, E.H. and Al-Tabbaa, A., 2017. Synthesis of reactive MgO from reject brine via the addition of NH<sub>4</sub>OH. *Hydrometallurgy*, 169: 165-172.

Dong, H.L., Unluer, C., Yang, E.H. and Al-Tabbaa, A., 2018. Recovery of reactive MgO from reject brine via the addition of NaOH. *Desalination*, 429: 88-95.

Dung, N. and Unluer, C., 2017a. Carbonated MgO concrete with improved performance: The influence of temperature and hydration agent on hydration, carbonation and strength gain. *Cement and Concrete Composites*.

Dung, N. and Unluer, C., 2017b. Sequestration of CO<sub>2</sub> in reactive MgO cement-based mixes with enhanced hydration mechanisms. *Construction and Building Materials*, 143: 71-82.

El-Naas, M.H., 2011. Reject brine management. INTECH Open Access Publisher.

Eubank, W.R., 1951. Calcination studies of magnesium oxides. *Journal of the American Ceramic Society*, 34(8): 225-229.

Fan, W. et al., 2004. Controlled synthesis of single-crystalline Mg(OH)<sub>2</sub> nanotubes and nanorods via a solvothermal process. *Journal of Solid State Chemistry*, 177(7): 2329-2338.

Fraunhofer, E., 2009. Developing Benchmarking Criteria for CO<sub>2</sub> Emissions. In: E.D.-G. European Commission, Service contract (Ed.).

Gao, P. et al., 2008. Production of MgO-type expansive agent in dam concrete by use of industrial by-products. *Building and Environment*, 43(4): 453-457.

Hanlon, J.M. et al., 2015. Rapid surfactant-free synthesis of Mg(OH)<sub>2</sub> nanoplates and pseudomorphic dehydration to MgO. *Crystengcomm*, 17(30): 5672-5679.

- Harrison, A.J.W., 2008. Reactive magnesium oxide cements.
- Hassan, D., 2013. Environmental Sustainability Assessment & Associated Experimental Investigations of Magnesia Production Routes, University of Cambridge.
- Henrist, C., Mathieu, J.-P., Vogels, C., Rulmont, A. and Cloots, R., 2003. Morphological study of magnesium hydroxide nanoparticles precipitated in dilute aqueous solution. *Journal of Crystal Growth*, 249(1): 321-330.
- Itatani, K., Itoh, A., Howell, F.S., Kishioka, A. and Kinoshita, M., 1993. Densification and microstructure development during the sintering of submicrometer magnesium-oxide particles prepared by a vapor-phase oxidation process. *Journal of Materials Science*, 28(3): 719-728.
- Itatani, K., Koizumi, K., Howell, F.S., Kishioka, A. and Kinoshita, M., 1988. Agglomeration of magnesium oxide particles formed by the decomposition of magnesium hydroxide .1. Agglomeration at increasing temperature. *Journal of Materials Science*, 23(9): 3405-3412.
- Itatani, K., Nomura, M., Kishioka, A. and Kinoshita, M., 1986. Sinterability of various high-purity magnesium-oxide powders. *Journal of Materials Science*, 21(4): 1429-1435.
- Jin, F. and Al-Tabbaa, A., 2014. Characterisation of different commercial reactive magnesia. *Advances in Cement Research*, 26(2): 101-113.
- Khuyen Thi, T., Han, K.S., Kim, S.J., Kim, M.J. and Tam, T., 2016. Recovery of magnesium from Uyuni salar brine as hydrated magnesium carbonate. *Hydrometallurgy*, 160: 106-114.
- Knibbs, N.V.S., 1924. Lime and magnesia.
- Kontoyannis, C.G. and Vagenas, N.V., 2000. Calcium carbonate phase analysis using XRD and FT-Raman spectroscopy. *The Analyst*, 125(2): 251-255.
- Lee, E.K., Jung, K.D., Joo, O.S. and Shul, Y.G., 2004. Magnesium oxide as an effective catalyst in catalytic wet oxidation of H<sub>2</sub>S to sulfur. *Reaction Kinetics and Catalysis Letters*, 82(2): 241-246.
- Liska, M., Al-Tabbaa, A., Carter, K. and Fifield, J., 2012a. Scaled-up commercial production of reactive magnesium cement pressed masonry units. Part I: Production. *Proceedings of the Institution of Civil Engineers-Construction Materials*, 165(4): 211-223.

Liska, M., Al-Tabbaa, A., Carter, K. and Fifield, J., 2012b. Scaled-up commercial production of reactive magnesia cement pressed masonry units. Part II: Performance. *Proceedings of the Institution of Civil Engineers-Construction Materials*, 165(4): 225-243.

Markov, I.V., 2016. *Crystal Growth for Beginners: Fundamentals of Nucleation, Crystal Growth and Epitaxy*. World Scientific Publishing Company.

Mo, L.W., Deng, M. and Tang, M.S., 2010. Effects of calcination condition on expansion property of MgO-type expansive agent used in cement-based materials. *Cement and Concrete Research*, 40(3): 437-446.

Mo, L.W., Deng, M., Tang, M.S. and Al-Tabbaa, A., 2014. MgO expansive cement and concrete in China: Past, present and future. *Cement and Concrete Research*, 57: 1-12.

Moussavi, G. and Mahmoudi, M., 2009a. Removal of azo and anthraquinone reactive dyes from industrial wastewaters using MgO nanoparticles. *Journal of Hazardous Materials*, 168(2-3): 806-812.

Moussavi, G. and Mahmoudi, M., 2009b. Removal of azo and anthraquinone reactive dyes from industrial wastewaters using MgO nanoparticles. *Journal of Hazardous Materials*, 168(2): 806-812.

Patterson, A.L., 1939. The Scherrer Formula for X-Ray Particle Size Determination. *Physical Review*, 56(10): 978-982.

Pilarska, A.A., Klapiszewski, Ł. and Jesionowski, T., 2017. Recent developments in the synthesis, modification and application of Mg(OH)<sub>2</sub> and MgO: A review. *Powder Technology*.

Ruan, S. and Unluer, C., 2016. Comparative life cycle assessment of reactive MgO and Portland cement production. *Journal of Cleaner Production*, 137: 258-273.

Shand, M.A., 2006. *The Chemistry and Technology of Magnesia*. Wiley.

Tran, K.T. et al., 2013. Recovery of magnesium from Uyuni salar brine as high purity magnesium oxalate. *Hydrometallurgy*, 138: 93-99.

Turek, M. and Gnot, W., 1995. Precipitation of magnesium hydroxide from brine. *Industrial & Engineering Chemistry Research*, 34(1): 244-250.

Unluer, C. and Al-Tabbaa, A., 2013. Impact of hydrated magnesium carbonate additives on the carbonation of reactive MgO cements. *Cement and Concrete Research*, 54: 87-97.

- Unluer, C. and Al-Tabbaa, A., 2014. Enhancing the carbonation of MgO cement porous blocks through improved curing conditions. *Cement and Concrete Research*, 59: 55-65.
- Wang, F., Jin, F., Shen, Z.T. and Al-Tabbaa, A., 2016. Three-year performance of in-situ mass stabilised contaminated site soils using MgO-bearing binders. *Journal of Hazardous Materials*, 318: 302-307.
- Wright, J.M. and Colling, A., 1995. *Seawater: Its Composition, Properties and Behaviour*. Elsevier Science.
- Wu, H., Shao, M., Gu, J. and Wei, X., 2004. Microwave-assisted synthesis of fibre-like Mg (OH) 2 nanoparticles in aqueous solution at room temperature. *Materials Letters*, 58(16): 2166-2169.
- Yan, C., Xue, D., Zou, L., Yan, X. and Wang, W., 2005. Preparation of magnesium hydroxide nanoflowers. *Journal of Crystal Growth*, 282(3): 448-454.